drones

MDPI

Article

QoS-Aware Deployment Optimization for Capsule Airport–UAV Emergency Communication Networks

Chaofeng Wang, Longfei Zhang *, Jie Luo and Shengming Dai

College of Airport, Civil Aviation Flight University of China, Deyang 618307, China
* Correspondence: zhanglongfei@cafuc.edu.cn

Highlights

What are the main findings?

- A QoS-aware joint optimization framework (QoS-TLK-VNS-K) is proposed for UAV deployment in capsule airport emergency communication networks. Statistical validation over 30 independent runs demonstrates significant improvements in QoS satisfaction (+23.8%, $p < 0.001$) and average SINR (+104.0%, $p < 0.001$) compared to the distance-based baseline.
- The interference–connectivity trade-off is systematically analyzed: increasing D_{int} from 300 m to 800 m generally improves average SINR (17.2 dB to 25.0 dB) while reducing sum rate (2579.7 Mbps to 1989.5 Mbps), with QoS satisfaction remaining stable between 46.0% and 53.8%, confirming that the default $D_{\text{int}} = 540$ m provides a balanced operating point.

What is the implication of the main finding?

- The proposed framework provides practical deployment guidelines for emergency communication network planners, enabling rapid and reliable UAV network establishment after natural disasters.
- The integrated optimization approach demonstrates that joint consideration of positioning, frequency allocation, and power control significantly outperforms decoupled optimization strategies in spectrum-constrained scenarios.

Abstract

When natural disasters strike, the destruction of terrestrial communication infrastructure creates urgent demands for emergency networks. Efficient UAV deployment in capsule airport–UAV hierarchical networks has emerged as a critical challenge due to limited aerial resources and stringent quality-of-service requirements. This paper develops a QoS-aware joint optimization model for UAV deployment, integrating air-to-ground (A2G) channel modeling with resource allocation, where upper-level position optimization is coordinated with lower-level frequency allocation and power control through a hierarchical decomposition strategy. The proposed QoS-TLK-VNS-K algorithm combines graph coloring for interference mitigation with iterative power control for SINR guarantee. Empirical evaluation using multi-scenario simulations demonstrates that the proposed approach significantly outperforms the traditional distance-based coverage method. Statistical validation over 30 independent runs demonstrates significant improvements in QoS satisfaction (+23.8%, $p < 0.001$), average SINR (+104.0%, $p < 0.001$), minimum user rate (+194.9%, $p < 0.001$), and Jain's fairness index (+16.2%, $p < 0.001$) compared to the distance-based baseline. These results demonstrate that the framework effectively addresses the trade-off between interference suppression and network connectivity in multi-UAV emergency communication systems.

Check for updates

Academic Editor: Filipe Pereira

Received: 31 May 2026
Revised: 7 July 2026
Accepted: 13 July 2026
Published: 16 July 2026

Copyright: © 2026 by the authors. Licensee MDPI, Basel, Switzerland. This article is an open access article distributed under the terms and conditions of the Creative Commons Attribution (CC BY) license.

Keywords: UAV; emergency communication; QoS-aware optimization; capsule airport; interference management; variable neighborhood search

1. Introduction

Natural disasters such as earthquakes, floods, and hurricanes cause widespread destruction to terrestrial communication infrastructure, severely disrupting emergency coordination and rescue operations. When base stations and fiber networks are damaged, affected populations lose access to critical communication services precisely when they are most needed—for emergency calls, disaster information dissemination, and coordination among rescue teams. The 2021 flooding disaster in Henan Province, China, exemplifies this vulnerability: 35,200 base stations (45% of the regional total) were disrupted in Zhengzhou city alone, leaving millions without communication access during the critical rescue window [1]. Unmanned aerial vehicle (UAV)-assisted communication networks, with their advantages of rapid deployment, flexible mobility, and low cost, have emerged as a key technological solution for emergency communication recovery [2–5].

The capsule airport (CA)–UAV hierarchical network represents an innovative architecture for emergency communications. CAs serve as mobile ground stations providing UAV takeoff/landing platforms, charging facilities, and backhaul connectivity, while UAVs function as aerial base stations serving ground users. This architecture encompasses three link types: air-to-ground (A2G) [6] links between UAVs and users, air-to-air (A2A) [7] links among UAVs for multi-hop backhaul, and UAV–CA (U2C) links for core network connectivity. The network architecture is illustrated in Figure 1.

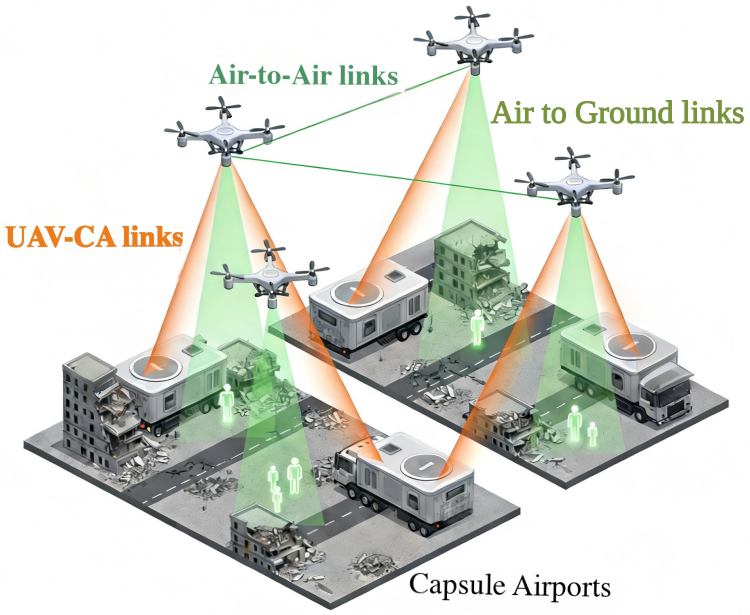


Figure 1. CA–UAV hierarchical emergency communication network architecture.

However, existing UAV deployment methods predominantly employ idealized geometric coverage models using distance-based criteria, neglecting actual communication quality constraints [8–10]. When multiple UAVs operate in proximity, co-channel interference severely degrades service quality, creating a gap between "geometric coverage" and "effective service". Jin et al. [8] developed the TLK-VNS-K algorithm for CA–UAV deployment, which provides an effective foundation for position optimization. However, the distance-based coverage criterion employed therein does not explicitly account for

co-channel interference, potentially leading to scenarios where geometrically covered users fail to achieve required SINR thresholds.

This observation motivates the development of a QoS-aware deployment framework that bridges the gap between geometric coverage and effective service quality. While joint optimization of UAV deployment and resource allocation has been explored in prior works [5,9], several aspects warrant further attention. First, many existing methods adopt simplified path loss models without probabilistic A2G channel characteristics, which may lead to optimistic SINR estimates. Second, interference management and position optimization are often treated as decoupled subproblems, with limited consideration of the mutual dependence between UAV topology and interference graph structure. Third, fairness among ground users is not always incorporated as an explicit optimization objective in multi-UAV emergency communication scenarios. Motivated by these observations, the proposed framework formulates a joint optimization problem over UAV positions, frequency allocation, and power control, which is then solved through a hierarchical decomposition strategy that coordinates position optimization with graph-coloring-based frequency allocation and iterative power control.

The main contributions of this paper are summarized as follows. (1) A QoS-aware deployment model incorporating probabilistic A2G channel characteristics and SINR-based coverage criteria is established. The fundamental trade-off between interference suppression (favoring larger UAV spacing) and A2A connectivity (requiring proximity for backhaul) is formally analyzed, providing theoretical guidance for algorithm design. (2) A joint optimization formulation integrating upper-level UAV position planning with lower-level resource allocation (frequency assignment and power control) is developed and formulated as a mixed-integer nonlinear program. To solve this computationally intractable problem efficiently, a hierarchical decomposition strategy is adopted that coordinates deployment decisions with interference management across sequential stages. (3) An enhanced VNS algorithm incorporating graph-coloring-based frequency allocation and iterative power control is designed to solve the formulated problem. The individual contribution of each module is isolated through an ablation study, and the overall performance gains are verified through statistical validation over multiple independent runs. The proposed method prioritizes effective QoS-satisfied service over geometric coverage count, consistent with the QoS-aware design objective.

The rest of the paper is organized as follows. Section 2 briefly reviews the related works. Section 3 presents the materials and methods, including the problem statement, system model, optimization formulation, and the QoS-TLK-VNS-K algorithm. Section 4 details the empirical evaluation encompassing multi-scenario simulations and sensitivity analysis. Section 6 concludes the paper and discusses future research directions.

2. Related Work

UAV-assisted communication network deployment has attracted significant research attention. This section reviews the relevant literature from five perspectives: coverage optimization, multi-UAV deployment, interference management, backhaul connectivity, and emergency communication applications.

2.1. Coverage Optimization

Coverage optimization constitutes a fundamental objective in UAV-assisted communication networks, aiming to maximize the number of ground users served by aerial base stations through optimal positioning strategies.

Mozaffari et al. [9] investigated optimal altitude determination for single UAV coverage maximization. Al-Hourani et al. [10,11] proposed the probabilistic line-of-sight (LoS)

channel model that establishes the relationship between UAV altitude and coverage probability, which has been widely adopted in subsequent research. Alzenad et al. [12] extended this framework to three-dimensional positioning optimization. Yuan et al. [13] investigated energy-efficient trajectory optimization for UAV-enabled cellular communications, jointly optimizing trajectory and power allocation to maximize secure energy efficiency.

These studies have established the foundational channel models and altitude–coverage relationships that underpin much of the subsequent UAV deployment literature. Building on these foundations, they are predominantly based on the assumption of interference-free single-UAV scenarios with distance-based coverage criteria, which may lead to optimistic performance estimates when extended to multi-UAV deployments where co-channel interference becomes nonnegligible.

2.2. Multi-UAV Cooperative Deployment

Multi-UAV cooperative deployment extends single-UAV optimization to coordinated swarm scenarios, addressing the joint challenges of position planning, load balancing, and inter-UAV coordination to achieve scalable and reliable coverage over large-scale disaster areas.

Wang et al. [14] studied multi-UAV deployment strategies that minimize the required number of UAVs while ensuring complete area coverage. Lyu et al. [15] employed spiral algorithms for sequential placement optimization. Sharma et al. [16] proposed clustering-based approaches that group users before determining UAV positions. Gowtham Raj and Bryan [17] addressed the UAV positioning problem using mixed-integer linear programming (MILP) to maximize user coverage, proposing a two-step clustering-then-optimization method that balances computational efficiency with solution optimality for large-scale scenarios. Jin et al. [8] addressed the CA–UAV hierarchical network through the 2L-MCDP-C&U problem formulation, designing TLK initialization combined with VNS-K optimization to achieve effective joint CA–UAV deployment. Recent advances in learning-based methods have also shown promise for cooperative deployment: Shi et al. [18] introduced symmetry-informed multi-agent reinforcement learning (MARL) for cooperative UAV swarm control in communication coverage tasks, exploiting spatial symmetry properties to enhance sample efficiency and scalability for large swarms with continuous control, and demonstrating superior performance over advanced baselines in handling up to 20 UAVs.

These studies have contributed effective strategies for coordinating multiple UAVs and have advanced scalable deployment over large areas. Building on these contributions, they are predominantly based on distance-based coverage criteria under the implicit assumption of orthogonal resource allocation among UAVs. This assumption may not hold in spectrum-constrained emergency scenarios, where frequency reuse among adjacent UAVs introduces co-channel interference that can degrade actual service quality below geometrically predicted levels.

2.3. Interference Management

Interference management addresses the signal quality degradation caused by co-channel transmissions among multiple UAVs, which becomes increasingly critical as deployment density grows to meet coverage demands in resource-constrained disaster scenarios.

Huang et al. [19] investigated interference coordination strategies in multi-tier UAV networks. Hydher et al. [20] proposed spectral efficiency-based deployment optimization that accounts for inter-cell interference effects. Recent advances have continued to address spectrum management challenges in multi-UAV coexistence scenarios: Shao et al. [21] proposed a joint bandwidth and spectrum usage zone allocation scheme

leveraging interference graph and graph coloring methods to maximize system utility in coexisting UAV networks, demonstrating that topology-aware frequency allocation significantly outperforms baseline schemes.

These studies have made valuable contributions to interference modeling and mitigation, establishing effective techniques for power control and spectrum sharing in multi-UAV networks. Beyond these works, recent studies have also explored interference-aware resource allocation and learning-based approaches for UAV network optimization. Building on these foundations, existing approaches are nonetheless generally based on simplified interference models or assume predetermined UAV positions, treating deployment and resource allocation as decoupled optimization problems. The joint consideration of UAV positioning, frequency assignment, and power control—where deployment decisions directly determine interference topology—has received comparatively less attention. As a result, the relationship between geometric coverage metrics and effective QoS-guaranteed service delivery remains an aspect that can be further strengthened.

2.4. Backhaul Connectivity

Backhaul connectivity ensures that UAVs can relay aggregated user traffic to the core network through A2A multi-hop links, which is essential for maintaining end-to-end communication quality in hierarchical aerial relay architectures.

Qiu et al. [22] studied joint access–backhaul optimization for UAV-assisted heterogeneous networks. Kalantari et al. [23] incorporated backhaul capacity constraints into UAV placement optimization, demonstrating the importance of considering backhaul limitations in deployment decisions.

These works have highlighted the importance of backhaul constraints in UAV placement and provided useful models for access–backhaul co-design. Building on these contributions, they predominantly model A2A backhaul links using distance-based connectivity constraints, assuming that link quality is guaranteed when UAVs are within communication range. However, under co-channel interference conditions, A2A links may experience quality degradation even when distance requirements are satisfied, potentially leading to backhaul bottlenecks or connectivity failures. The fundamental trade-off between interference suppression (which favors larger inter-UAV spacing) and connectivity maintenance (which requires proximity for reliable A2A links) has received limited systematic analysis in the existing literature.

2.5. Emergency Communication Applications

Emergency communication represents a primary application context for UAV-assisted networks, where rapid deployment capability and service reliability are paramount for effective disaster response and relief coordination.

Recent research has increasingly focused on UAV deployment optimization for emergency scenarios. Saeed et al. [24] proposed a UAV computing-assisted framework for search and rescue missions in disaster environments, evaluating network performance metrics including delay, throughput, and path loss to demonstrate the effectiveness of UAV-assisted intelligent edge computing for emergency data exchange. Shah [25] developed a cluster-based Flying Ad Hoc Network (FANET) architecture for emergency communication systems in 5G and beyond, proposing a novel backoff mechanism based on cluster size to optimize performance under high node mobility conditions. More recently, Loor-Duque et al. [26] proposed a lightweight machine-learning-based QoS optimization framework for multi-UAV emergency communications in FANETs, combining realistic mobility modeling with adaptive traffic prioritization and demonstrating approximately

43% improvement in packet delivery ratio and 70% reduction in end-to-end delay over baseline schemes.

These studies demonstrate the practical value of optimized UAV deployment in emergency communication contexts and provide effective frameworks for disaster-response scenarios. They primarily focus on coverage efficiency and deployment cost, while the interference–connectivity trade-off that arises when multiple UAVs operate in proximity under spectrum-constrained conditions receives comparatively less explicit attention.

In summary, Table 1 presents a comprehensive comparison of existing approaches across key technical dimensions, highlighting the research gaps addressed by this paper.

Table 1. Comparative analysis of related works.

Reference	Multi-UAV Deployment	SINR-Based Coverage	Frequency Allocation	Power Control	Backhaul Model	Trade-Off Analysis
Mozaffari [9]	✗	✗	✗	✗	✗	✗
Al-Hourani [11]	✗	✗	✗	✗	✗	✗
Lyu [15]	✓	✗	✗	✗	✗	✗
Gowtham Raj [17]	✓	✗	✗	✗	✗	✗
Jin [8]	✓	✗	✗	✗	✓	✗
Huang [19]	✓	Partial	✓	✗	✗	✗
Hydher [20]	✓	Partial	✗	✓	✗	✗
Qiu [22]	✓	✗	✗	✗	✓	✗
Kalantari [23]	✓	✗	✗	✗	✓	✗
Saeed [24]	✓	✗	✗	✗	✗	✗
Shah [25]	✓	✗	✗	✗	✗	✗
This paper	✓	✓	✓	✓	✓	✓

Classification criteria: ✓ (Addressed)—the dimension is explicitly modeled and incorporated into the method's optimization or constraints; Partial—the dimension is considered qualitatively or under simplifying assumptions without an explicit guarantee (e.g., SINR is used for evaluation but not enforced as a per-user constraint); ✗ (Not addressed)—the dimension is not considered. The table is intended to position the proposed work relative to prior art rather than to provide an exhaustive evaluation.

In summary, as shown in Table 1, existing works address UAV deployment and resource allocation largely in isolation, exhibiting three principal gaps: most approaches rely on distance-based coverage criteria without SINR-based QoS constraints; deployment and resource allocation are typically treated as decoupled problems; and the fundamental trade-off between interference suppression and network connectivity has not been systematically analyzed. The proposed QoS-TLK-VNS-K algorithm differs from prior art in three respects: (1) it jointly optimizes UAV positions and resource allocation in a tightly coupled bilevel structure where position updates trigger immediate resource reallocation; (2) it employs graph coloring to exploit the interference topology for frequency assignment, rather than using fixed or random channel allocation; and (3) it explicitly incorporates per-user SINR constraints and fairness into the deployment objective, so that the reported coverage more closely reflects QoS-satisfied service.

3. Materials and Methods

3.1. Problem Statement

An emergency communication network is deployed consisting of M capsule airports (CAs) and N UAVs to serve K ground users.

Existing deployment methods, exemplified by Jin et al.'s TLK-VNS-K algorithm [8], optimize UAV positions to maximize the number of geometrically covered users (i.e., users within distance R_{cov} from any UAV). However, this approach exhibits three critical lim-

itations. First, all UAVs operate on the same frequency channel, causing severe co-channel interference, and users near cell boundaries experience SINR below required thresholds despite being within coverage distance. Second, the gap between geometric coverage and effective service leads to "false coverage"—users counted as covered but unable to achieve satisfactory communication quality. Third, air-to-air links for multi-hop backhaul may fail under interference, potentially disconnecting remote UAVs from the core network.

As an illustrative example, consider a scenario with 100 users and 6 UAVs. Under the TLK-VNS-K approach, 73 users are geometrically covered, but only 48 users (65.8%) achieve SINR $\geq$ 10 dB threshold. This 25-user gap represents false coverage caused by unmanaged interference.

This paper aims to develop a QoS-aware deployment framework that (1) replaces distance-based coverage with SINR-based QoS criteria; (2) jointly optimizes UAV positions, frequency allocation, and power control; and (3) balances interference suppression with network connectivity requirements. Following the complementary relationship with Jin et al. [8], CA locations are selected from a set of predetermined candidate sites that satisfy terrain and accessibility constraints (e.g., elevated, flat, and disaster-safe positions), and the selection is performed by the two-layer K-means initialization. This paper then focuses on UAV deployment and resource optimization given the selected CA locations; the joint optimization of CA siting together with QoS-aware UAV deployment is discussed as a direction for future work in Section 6.

3.2. System Model

This subsection presents the system model for the capsule airport–UAV hierarchical emergency communication network. For clarity, all symbols are summarized in Table 2, to which the reader is referred for any symbol used below; each key variable is also defined in the text at or before its first use. The model is built up in the following order: network components, the air-to-ground (A2G) and air-to-air (A2A) channel models, the SINR computation, the QoS-aware coverage criterion, and the backhaul connectivity model.

Table 2. Summary of notation. Algorithm-specific parameters (e.g., $k_{\max}$, I_{VNS}, Δ_{margin}, δ_p, I_{pc}, D_{int}) are listed separately in Table 4.

Category	Symbol	Definition
Sets	$\mathcal{M}$	Set of capsule airports, $\lvert\mathcal{M}\rvert = M$
	$\mathcal{N}$	Set of UAVs, $\lvert\mathcal{N}\rvert = N$
	$\mathcal{K}$	Set of ground users, $\lvert\mathcal{K}\rvert = K$
	$\mathcal{F}$	Set of frequency channels, $\lvert\mathcal{F}\rvert = F_{\max}$
Positions	$\mathbf{c}_m$	Position of CA m
	$\mathbf{u}_n = (x_n, y_n, h_n)$	3D position of UAV n
	$\mathbf{w}_k$	Position of user k
	$h_n \in [H_{\min}, H_{\max}]$	Altitude of UAV n (m)
Channel	P_{LoS}	Line-of-sight probability
	$\overline{PL}_{n,k}$	Average path loss (dB)
	$g_{n,k}$	Channel power gain
	$\theta_{n,k}$	Elevation angle (degrees)
	f_c	Carrier frequency
	$\eta_{\text{LoS}}, \eta_{\text{NLoS}}$	LoS/NLoS excess path loss (dB)
	a, b	Environment-dependent S-curve parameters

Table 2. *Cont.*

Category	Symbol	Definition
Resources	P_n	Transmit power of UAV n (W)
	$f_n \in \mathcal{F}$	Frequency channel of UAV n
	$a_{k,n} \in \{0,1\}$	User–UAV association indicator
	$b_{n,m} \in \{0,1\}$	UAV–CA assignment indicator
	$P_{\min}, P_{\max}$	Minimum/maximum transmit power
	B, B_k	Total/per-user bandwidth
	σ^2, N_0	Noise power/noise PSD
Performance	γ_k	SINR of user k (linear scale)
	R_k	Achievable rate of user k (bps)
	γ_{th}	SINR threshold (dB)
	$\mathcal{K}_{\text{served}}$	Set of QoS-satisfied served users
	$R_{\text{sum}}, R_{\min}$	Sum rate/minimum user rate
Parameters	R_{cov}	UAV coverage radius (m)
	R_{CA}	CA communication radius (m)
	$C_{\max}$	UAV maximum user capacity
	D_{int}	Interference distance threshold (m)
	$H_{\min}, H_{\max}$	Minimum/maximum UAV altitude (m)
	H_{opt}	Optimal UAV altitude (m)
	D_{A2A}	Maximum A2A communication range (m)
	$\gamma_{\text{th}}^{\text{A2A}}$	A2A SINR threshold (dB)

3.2.1. Network Components

Consider a disaster area $\mathcal{A} \subset \mathbb{R}^2$ with K ground users and N UAVs serving them through M capsule airports. Let $\mathcal{K} = \{1, 2, \ldots, K\}$ denote the set of users with positions $\{\mathbf{w}_k\}_{k\in\mathcal{K}}$, where $\mathbf{w}_k = (x_k^w, y_k^w, 0)$. Let $\mathcal{M} = \{1, 2, \ldots, M\}$ denote the set of CAs with positions $\{\mathbf{c}_m\}_{m\in\mathcal{M}}$. Let $\mathcal{N} = \{1, 2, \ldots, N\}$ denote the set of UAVs to be deployed at positions $\{\mathbf{u}_n\}_{n\in\mathcal{N}}$, where $\mathbf{u}_n = (x_n, y_n, h_n)$ with adjustable altitude $h_n \in [H_{\min}, H_{\max}]$. The system operates on a set of $F_{\max}$ orthogonal frequency channels $\mathcal{F} = \{1, 2, \ldots, F_{\max}\}$ with total bandwidth B. Each UAV n is assigned a frequency channel $f_n \in \mathcal{F}$, transmits with power $P_n \in [P_{\min}, P_{\max}]$, and serves at most $C_{\max}$ users simultaneously.

Let $\mathcal{K}_n = \{k \in \mathcal{K} \mid a_{k,n} = 1\}$ denote the set of users associated with UAV n, where $a_{k,n} \in \{0, 1\}$ is the user–UAV association indicator. A user k is considered *QoS-satisfied* if its received SINR exceeds the threshold γ_{th}, i.e., $\gamma_k \geq \gamma_{\text{th}}$.

3.2.2. A2G Channel Model

This paper adopts the Al-Hourani probabilistic line-of-sight (LoS) model [10,11]. The channel characteristics are described by the following equations:

$$P_{\text{LoS}}(\theta_{n,k}) = \frac{1}{1 + a \cdot \exp(-b(\theta_{n,k} - a))}, \tag{1}$$

$$\theta_{n,k} = \frac{180}{\pi} \cdot \arctan\left(\frac{h_n}{r_{n,k}}\right), \tag{2}$$

$$r_{n,k} = \sqrt{(x_n - x_k^w)^2 + (y_n - y_k^w)^2}, \tag{3}$$

where Equation (1) represents the LoS probability as a function of elevation angle, Equation (2) defines the elevation angle $\theta_{n,k}$ (in degrees) between UAV n and user k, and Equation (3) computes the horizontal distance $r_{n,k}$. Parameters a and b are environment-dependent constants (urban environment: $a = 9.61$, $b = 0.16$).

The average path loss incorporating both LoS and NLoS components is given by

$$\overline{PL}_{n,k} = PL_{\text{free}}(d_{n,k}) + P_{\text{LoS}} \cdot \eta_{\text{LoS}} + (1 - P_{\text{LoS}}) \cdot \eta_{\text{NLoS}}, \tag{4}$$

$$PL_{\text{free}}(d) = 20 \log_{10}\left(\frac{4\pi f_c d}{c}\right), \tag{5}$$

$$d_{n,k} = \sqrt{r_{n,k}^2 + h_n^2}, \tag{6}$$

where PL_{free} denotes the free-space path loss, $d_{n,k}$ is the three-dimensional Euclidean distance, f_c is the carrier frequency, c is the speed of light, and $\eta_{\text{LoS}} = 1.0$ dB and $\eta_{\text{NLoS}} = 20.0$ dB represent additional attenuation factors for LoS and NLoS conditions, respectively.

3.2.3. A2A Link Model

For air-to-air communication between UAVs, line-of-sight (LoS) propagation is assumed due to the elevated positions and unobstructed paths, consistent with the air-to-air channel modeling adopted in Jin et al. [8]. The A2A path loss follows the standard free-space model and is given by

$$PL_{i,j}^{\text{A2A}} = 20 \log_{10}\left(\frac{4\pi f_c d_{i,j}}{c}\right) + \eta_{\text{LoS}}, \tag{7}$$

$$d_{i,j} = \left\|\mathbf{u}_i - \mathbf{u}_j\right\|_2 = \sqrt{(x_i - x_j)^2 + (y_i - y_j)^2 + (h_i - h_j)^2}, \tag{8}$$

where $d_{i,j}$ denotes the three-dimensional distance between UAV i and UAV j, and $\mathbf{u}_i = (x_i, y_i, h_i)$ represents the position vector of UAV i.

3.2.4. SINR Computation

The received signal quality is characterized by the signal-to-interference-plus-noise ratio (SINR). While the underlying path-loss models are adopted from the literature (the Al-Hourani A2G model [10,11] and the standard free-space A2A model), the explicit incorporation of co-channel interference into the SINR—rather than relying solely on a distance- or path-loss-based connectivity criterion as in [8]—is a distinguishing feature of the proposed QoS-aware formulation. For user k associated with UAV n, the downlink SINR is

$$\gamma_k = \frac{P_n \cdot g_{n,k}}{\sum_{j \in \mathcal{N}, j \neq n, f_j = f_n} P_j \cdot g_{j,k} + \sigma^2}, \tag{9}$$

$$g_{n,k} = 10^{-\overline{PL}_{n,k}/10}, \tag{10}$$

$$\sigma^2 = N_0 \cdot B, \tag{11}$$

where P_n denotes the transmit power of UAV n, $g_{n,k}$ is the channel power gain derived from the average path loss, σ^2 is the additive white Gaussian noise (AWGN) power, N_0 is the noise power spectral density, and B is the channel bandwidth. The summation in the denominator accounts for co-channel interference from UAVs operating on the same frequency channel f_n. Unless otherwise stated, γ_k denotes the SINR in linear scale, as required by the achievable-rate expression in Equation (20); SINR values reported in decibels throughout the experimental section are obtained as $10 \log_{10}(\gamma_k)$ for presentation purposes.

Similarly, the SINR for the A2A link from UAV i to UAV j is

$$\gamma_{i,j}^{\mathrm{A2A}} = \frac{P_i \cdot g_{i,j}^{\mathrm{A2A}}}{\sum_{l \in \mathcal{N}, l \neq i, f_l = f_i} P_l \cdot g_{l,j}^{\mathrm{A2A}} + \sigma^2}, \tag{12}$$

$$g_{i,j}^{\mathrm{A2A}} = 10^{-PL_{i,j}^{\mathrm{A2A}}/10}, \tag{13}$$

where P_i and P_l denote the transmit powers of UAVs i and l, respectively, following the same notation P_n defined for a generic UAV n in Table 2 (the subscript merely indexes different UAVs); $g_{i,j}^{\mathrm{A2A}}$ is the A2A channel power gain, and the interference term captures transmissions from other UAVs utilizing the same frequency channel.

Two simplifying assumptions are made in the interference model. First, only co-channel interference is considered: UAVs operating on different frequency channels are assumed to be orthogonal, and adjacent-channel interference is neglected. This is a common assumption when channels are well separated in frequency, and it is reasonable here because the graph-coloring allocation assigns distinct channels to mutually interfering UAVs. Second, the model adopts a full-buffer, fully-loaded interference assumption in which all co-channel UAVs are treated as simultaneously active, without explicit time-slot scheduling among links; this represents a worst-case interference condition and therefore yields conservative SINR estimates. Incorporating adjacent-channel leakage and finer-grained inter-link scheduling is a possible direction for future refinement.

3.2.5. QoS Coverage Criterion

Unlike traditional distance-based coverage, this paper defines QoS-aware coverage based on SINR satisfaction:

$$\mathcal{C}_n^{\mathrm{dist}} = \{k \in \mathcal{K} \mid r_{n,k} \leq R_{\mathrm{cov}}\}, \tag{14}$$

$$\mathcal{C}_n^{\mathrm{QoS}} = \left\{k \in \mathcal{C}_n^{\mathrm{dist}} \mid \gamma_k \geq \gamma_{\mathrm{th}}\right\}, \tag{15}$$

where Equation (14) defines the set of users within geometric coverage radius R_{cov} of UAV n, and Equation (15) further restricts this set to users satisfying the SINR threshold γ_{th}. The difference $|\mathcal{C}_n^{\mathrm{dist}}| - |\mathcal{C}_n^{\mathrm{QoS}}|$ quantifies the "false coverage"—users that are geometrically covered but fail to meet the SINR requirement. The underlying mismatch between geometric coverage and effective signal quality has been recognized in interference-aware UAV deployment studies [19,20], where SINR or spectral-efficiency considerations are incorporated into placement. However, this gap is seldom quantified explicitly as a deployment-level metric in multi-UAV emergency scenarios; in this work we make it explicit by separately reporting geometric coverage and QoS-satisfied coverage, and by treating their difference as a measure of false coverage.

The system-level performance metrics are defined as

$$\eta_{\mathrm{cov}} = \frac{\left|\bigcup_{n \in \mathcal{N}} \mathcal{C}_n^{\mathrm{dist}}\right|}{K} \times 100\%, \tag{16}$$

$$\eta_{\mathrm{QoS}} = \frac{\left|\bigcup_{n \in \mathcal{N}} \mathcal{C}_n^{\mathrm{QoS}}\right|}{K} \times 100\%, \tag{17}$$

where η_{cov} and η_{QoS} represent the coverage ratio and QoS satisfaction ratio, respectively.

3.2.6. Backhaul Connectivity Model

To ensure end-to-end communication, each UAV must maintain backhaul connectivity to the core network through CAs. The A2A communication topology is modeled as an undirected graph $\mathcal{G}_{\text{A2A}} = (\mathcal{N}, \mathcal{E}_{\text{A2A}})$, where the edge set is defined as

$$\mathcal{E}_{\text{A2A}} = \left\{(i,j) \mid d_{i,j} \leq D_{\text{A2A}} \text{ and } \gamma_{i,j}^{\text{A2A}} \geq \gamma_{\text{th}}^{\text{A2A}},\ i,j \in \mathcal{N},\ i \neq j\right\}, \tag{18}$$

with D_{A2A} being the maximum A2A communication range and $\gamma_{\text{th}}^{\text{A2A}}$ the minimum SINR threshold for reliable A2A links.

Similarly, the UAV-to-CA (U2C) connectivity is captured by edge set $\mathcal{E}_{\text{U2C}}$, where $(n,m) \in \mathcal{E}_{\text{U2C}}$ if UAV n can directly communicate with CA m. The backhaul connectivity graph is defined as

$$\mathcal{G}_B = (\mathcal{N} \cup \mathcal{M},\ \mathcal{E}_{\text{A2A}} \cup \mathcal{E}_{\text{U2C}}), \tag{19}$$

which must be connected to ensure all UAVs have paths to the core network.

3.3. Trade-Off Analysis: Interference vs. Connectivity

A fundamental trade-off exists between interference suppression and network connectivity, as illustrated in Figure 2. When UAVs are deployed with small inter-UAV spacing, strong A2A links (represented by thick solid lines) enable robust backhaul connectivity, allowing reliable data transmission between UAVs and to the ground stations. However, this close proximity results in significant overlap of coverage areas (shown as overlapping circles on the ground), creating severe co-channel interference that degrades the quality of service for users located in the overlapping regions, particularly those at cell boundaries.

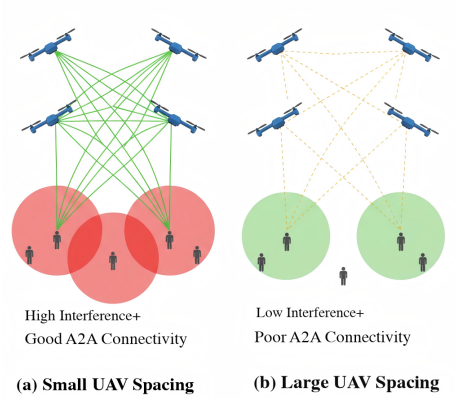


Figure 2. Illustration of the interference–connectivity trade-off: (**a**) small UAV spacing with high interference but good A2A connectivity; (**b**) large UAV spacing with low interference but poor A2A connectivity.

Conversely, when UAVs are positioned with large spatial separation, the coverage areas are well separated with minimal overlap, effectively eliminating co-channel interference and ensuring high-quality service for ground users. Nevertheless, the increased distances result in weakened A2A links (depicted by thin dashed lines), which may fail to meet minimum SINR requirements for reliable backhaul communication, potentially causing network fragmentation and isolating remote UAVs from the core network infrastructure.

To ensure user QoS, co-channel interference must be minimized, which favors larger UAV spacing, lower transmit power, and different frequency channels for adjacent UAVs. Conversely, to maintain backhaul connectivity, A2A links must satisfy SINR thresholds, which favors smaller UAV spacing, higher transmit power, and connected topology in the backhaul graph. These requirements conflict directly, as summarized in Table 3.

Table 3. Conflicting requirements between interference suppression and connectivity.

Requirement	UAV Spacing	Transmit Power
Interference suppression	Increase ↑	Decrease ↓
Network connectivity	Decrease ↓	Increase ↑

This paper resolves the trade-off through two mechanisms. First, graph coloring frequency allocation assigns different frequencies to adjacent UAVs, eliminating co-channel interference without requiring increased spacing. Second, iterative power control reduces transmit power after interference elimination while maintaining QoS, further improving system performance.

3.4. Optimization Model

3.4.1. Decision Variables

The optimization involves the following decision variables:

- UAV positions: $\mathbf{U} = \{(x_n, y_n, h_n)\}_{n=1}^{N}$, where (x_n, y_n) is the horizontal position and h_n is the altitude;
- User association: $\mathbf{A} = \{a_{k,n}\} \in \{0,1\}^{K \times N}$, where $a_{k,n} = 1$ indicates user k is served by UAV n;
- Frequency allocation: $\mathbf{F} = \{f_n\}_{n=1}^{N}$ with $f_n \in \mathcal{F} = \{1, \ldots, F_{\max}\}$;
- Power control: $\mathbf{P} = \{P_n\}_{n=1}^{N}$ with $P_n \in [P_{\min}, P_{\max}]$.

3.4.2. Objective Functions

Before defining the objectives, we clarify the role of QoS satisfaction in the proposed formulation. Rather than appearing as a term in the objective function, the per-user SINR requirement acts as an admission constraint (C2): only users whose received SINR meets the threshold γ_{th} are counted as served and enter the served-user set $\mathcal{K}_{\text{served}} = \bigcup_{n \in \mathcal{N}} \mathcal{C}_n^{\text{QoS}}$. All objective functions below are then defined exclusively over this QoS-satisfied set. Consequently, "QoS-aware" in this work means that optimization is performed only over users that genuinely satisfy the quality requirement, rather than maximizing a count of geometrically covered users. This design also explains why the QoS satisfaction ratio equals the coverage ratio for the proposed method (Section 4.2): a user is counted as covered only if it is QoS-satisfied. Treating QoS as a gating constraint, rather than as an objective term, keeps the objective functions well defined in standard throughput and fairness units while guaranteeing that every served user meets the SINR requirement. Let $\mathcal{K}_{\text{served}} = \bigcup_{n \in \mathcal{N}} \mathcal{C}_n^{\text{QoS}}$ denote the set of users that are both geometrically covered and satisfy the SINR requirement. The achievable data rate of user k is given by

$$R_k = B_k \log_2(1 + \gamma_k), \tag{20}$$

where B_k denotes the bandwidth allocated to user k. For tractability, equal bandwidth allocation is assumed, i.e., $B_k = B/|\mathcal{K}_n|$ for $k \in \mathcal{C}_n^{\text{QoS}}$, where B is the total channel bandwidth per UAV. This assumption isolates the effect of the three decision dimensions considered in this work—UAV position, frequency allocation, and power control—from that of intra-cell bandwidth scheduling, keeping the optimization focused and the per-user rate well defined. Under equal allocation, the sum rate and fairness metrics reflect differences in SINR and user-load distribution rather than in bandwidth assignment; incorporating nonuniform, QoS-aware bandwidth allocation as an additional decision variable is a natural extension left for future work.

Three objective functions are considered to address different optimization goals:

(1) Sum rate maximization. This objective maximizes the aggregate system throughput:

$$\max_{\mathbf{U},\mathbf{A},\mathbf{F},\mathbf{P}} \quad R_{\text{sum}} = \sum_{k \in \mathcal{K}_{\text{served}}} R_k = \sum_{k \in \mathcal{K}_{\text{served}}} B_k \log_2(1 + \gamma_k). \tag{21}$$

(2) Max–min fairness. This objective maximizes the minimum user rate to ensure equitable service distribution:

$$\max_{\mathbf{U},\mathbf{A},\mathbf{F},\mathbf{P}} \quad R_{\min} = \min_{k \in \mathcal{K}_{\text{served}}} R_k. \tag{22}$$

(3) Hybrid objective. This objective balances throughput and fairness through a weighted combination:

$$\max_{\mathbf{U},\mathbf{A},\mathbf{F},\mathbf{P}} \quad \alpha \cdot \frac{R_{\text{sum}}}{R_{\text{sum}}^{\text{ref}}} + (1 - \alpha) \cdot \frac{R_{\min}}{R_{\min}^{\text{ref}}}, \tag{23}$$

where $\alpha \in [0, 1]$ is the weight parameter controlling the trade-off between sum rate and fairness. The reference values $R_{\text{sum}}^{\text{ref}}$ and $R_{\min}^{\text{ref}}$ are the sum rate and minimum user rate achieved by the initial TLK-VNS-K solution for the same problem instance, and serve as normalization constants so that both terms in Equation (23) are dimensionless and of comparable magnitude. They are therefore instance-dependent but fixed once the initialization is computed, so they do not vary during the optimization. As both terms are normalized to the same baseline, the relative weighting is governed solely by α, whose sensitivity is examined in Section 4.5.2.

These three objectives represent alternative formulations of the deployment problem rather than simultaneously optimized criteria: each defines a distinct single-objective problem solved independently, and the operator selects one according to the deployment priority (aggregate throughput, worst-case fairness, or a balance of both). The sum rate objective is used as the default in all subsequent experiments unless otherwise stated, as it provides the most direct comparison with the coverage-oriented objective of the TLK-VNS-K baseline; the effect of the objective choice is analyzed in Section 4.5.2.

3.4.3. Constraints

The optimization problem is subject to the following constraints:

C1 (Coverage distance):

$$r_{n,k} \leq R_{\text{cov}}, \quad \forall k \in \mathcal{K}_n, \forall n \in \mathcal{N}, \tag{24}$$

where R_{cov} is the maximum service radius of each UAV.

C2 (SINR requirement):

$$\gamma_k \geq \gamma_{\text{th}}, \quad \forall k \in \mathcal{K}_{\text{served}}. \tag{25}$$

C3 (UAV capacity):

$$|\mathcal{K}_n| \leq C_{\max}, \quad \forall n \in \mathcal{N}. \tag{26}$$

C4 (Single UAV association):

$$\sum_{n \in \mathcal{N}} a_{k,n} \leq 1, \quad \forall k \in \mathcal{K}. \tag{27}$$

C5 (Altitude bounds):

$$H_{\min} \leq h_n \leq H_{\max}, \quad \forall n \in \mathcal{N}. \tag{28}$$

C6 (Power bounds):

$$P_{\min} \leq P_n \leq P_{\max}, \quad \forall n \in \mathcal{N}. \tag{29}$$

C7 (A2A link quality):

$$\gamma_{i,j}^{\text{A2A}} \geq \gamma_{\text{th}}^{\text{A2A}}, \quad \forall (i,j) \in \mathcal{E}_{\text{A2A}}. \tag{30}$$

C8 (Backhaul connectivity):

$$\mathcal{G}_B \text{ is connected, i.e., each UAV has a path to at least one CA.} \tag{31}$$

3.4.4. Problem Formulation Summary

Combining the objective functions and constraints, the QoS-aware UAV deployment problem can be formulated as follows:

$$\begin{aligned} \mathcal{P}: \quad & \max_{\mathbf{U},\mathbf{A},\mathbf{F},\mathbf{P}} \quad \text{Objective: (21), (22), or (23)} \\ & \text{s.t.} \quad \text{C1–C8: Equations (24)–(31).} \end{aligned} \tag{32}$$

Problem $\mathcal{P}$ is a mixed-integer nonlinear program (MINLP) due to the discrete frequency allocation, binary user association, and nonlinear SINR expressions. The coupling between UAV positions and interference topology further increases computational complexity. To address this, we propose a hierarchical algorithm that decomposes the problem into manageable subproblems.

3.5. Algorithms

3.5.1. Overall Solution Framework

The proposed QoS-TLK-VNS-K algorithm adopts a hierarchical optimization structure with four sequential phases:

1. Phase 1 (Initialization): TLK algorithm generates initial UAV positions and CA assignments;
2. Phase 2 (Position Optimization): VNS framework optimizes UAV horizontal positions;
3. Phase 3 (Resource Allocation): Graph coloring allocates frequencies and iterative algorithm controls power;
4. Phase 4 (Refinement): Altitude optimization and connectivity verification.

Although the optimization problem is formulated jointly, it is solved through a hierarchical decomposition for computational tractability. The interaction between modules is designed around a key principle: position updates and resource reallocation are tightly coordinated within this decomposition. Specifically, after each VNS position perturbation (Phase 2), graph coloring and power control are immediately reinvoked to compute the resource allocation consistent with the new UAV topology. This ensures that the objective function evaluation always reflects the actual achievable QoS under optimal resource allocation for the current positions, rather than using stale resource assignments from previous iterations.

The coupling mechanism prevents a common failure mode in decoupled approaches: a position update that improves geometric coverage may simultaneously worsen interference topology, leading to lower actual QoS. By re-evaluating resources after every position change, the VNS search receives accurate feedback and converges to solutions that are jointly optimal in both position and resource dimensions.

The TLK initialization (Phase 1) seeds the VNS with a high-quality starting point, reducing the risk of the search being trapped in poor local optima. The two-layer K-means structure ensures that UAVs are initially distributed to cover both CA service areas and user

clusters, providing a geometrically sound starting configuration from which QoS-aware refinement proceeds. The graph coloring (Phase 3) and power control (Phase 4) modules then translate this geometric foundation into guaranteed signal quality by eliminating co-channel interference and satisfying per-user SINR constraints.

It is important to clarify the relationship between the problem formulation and the solution strategy. The optimization problem in Section 3.4 is formulated jointly over UAV positions, user association, frequency allocation, and power control, and is a mixed-integer nonlinear program whose direct joint solution is computationally intractable at the scale of emergency deployment. The proposed QoS-TLK-VNS-K therefore solves this problem through a hierarchical decomposition rather than a fully simultaneous optimization. This design choice is motivated by tractability: decoupling the discrete position search from the resource-allocation subproblems reduces the search space from the full joint space to a sequence of manageable subproblems, enabling solutions within seconds (Section 4.3).

We acknowledge that such decomposition does not guarantee global optimality of the original joint problem: decisions made in the position stage constrain the feasible space of the subsequent frequency and power stages. To mitigate this loss, the proposed strategy does not execute the stages in a single forward pass; instead, frequency allocation and power control are reinvoked after every position perturbation within the VNS loop (Algorithm 3, Lines 14–19), so that each candidate position is evaluated under its own optimal resource allocation. This feedback coupling distinguishes the proposed approach from a purely sequential pipeline, as each position is assessed together with its corresponding resource allocation rather than under fixed assignments, while retaining the tractability of decomposition. A fully integrated solution, for example, via learning-based or exact MINLP methods, is left as future work.

The algorithm flowchart is shown in Figure 3.

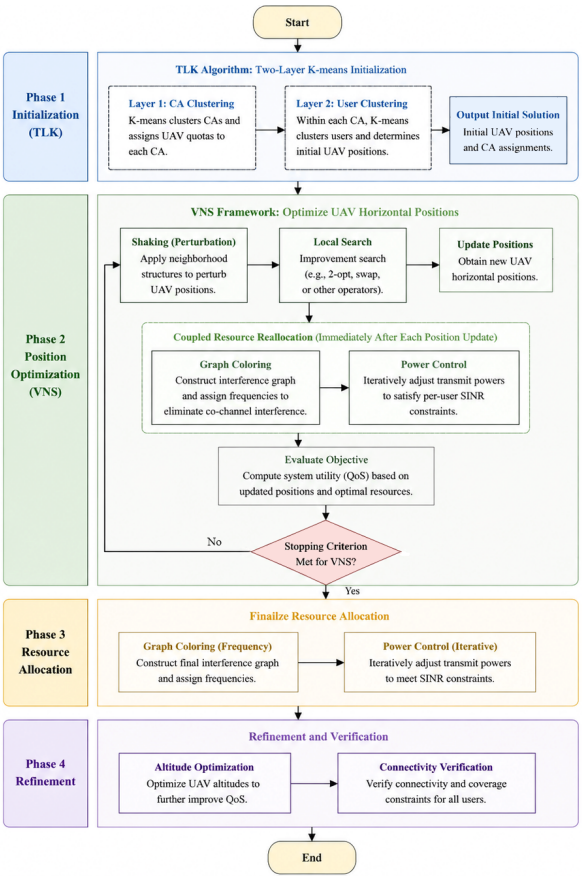


Figure 3. QoS-TLK-VNS-K algorithm flowchart.

3.5.2. TLK Initialization

The two-layer K-means (TLK) algorithm [8] generates initial solutions through a two-stage clustering process:

- Layer 1: Partitions users into M groups based on nearest CA assignment;
- Layer 2: Applies K-means clustering within each CA's user subset to determine UAV positions.

Let $\mathbf{B} = \{b_n\}_{n \in \mathcal{N}}$ denote the CA assignment vector, where $b_n \in \mathcal{M}$ indicates which CA is responsible for UAV n. Following Jin et al. [8], all UAVs are initially placed at the optimal altitude that maximizes the coverage radius under the Al-Hourani air-to-ground channel model [10,11]. Given the urban environment parameters ($a = 9.61$, $b = 0.16$) and the path-loss threshold, this optimal altitude is obtained by locating the inflection point of the coverage-radius-versus-altitude relationship, yielding $H_{\text{opt}} = 178$ m with a corresponding maximum coverage radius $R_{\text{cov}} = 270$ m.

3.5.3. VNS Position Optimization

Variable neighborhood search (VNS) systematically explores the solution space through multiple neighborhood structures. Let $k_{\max}$ denote the maximum number of neighborhood structures. The following neighborhoods are defined:

- $\mathcal{N}_1$ (Centroid Move): Moves UAV to the centroid of its served users;
- $\mathcal{N}_2$ (Random Perturbation): Perturbs position within radius $r_k = 50k$ m, where k is the neighborhood index
- $\mathcal{N}_3$ (Swap): Exchanges positions of two UAVs;
- $\mathcal{N}_4$ (Reassignment): Reassigns a UAV to a different CA.

The VNS procedure iterates until convergence or reaching the maximum iterations I_{VNS}. A patience parameter controls early stopping: if no improvement is found for patience consecutive iterations, the algorithm terminates. Because the TLK initialization provides the starting point for the VNS search, the quality of the initial deployment can, in principle, influence the final solution. The VNS framework is specifically designed to mitigate this dependence: the shaking operators perturb the incumbent solution across neighborhood structures of increasing size, enabling the search to escape the local optimum associated with the initial configuration, while the local-search operators refine the perturbed solutions. The empirical effect of this design is reflected in the statistical validation (Section 4.7): across 30 independent runs with different random seeds—and therefore different user distributions and different TLK initial solutions—the proposed method exhibits a small standard deviation in QoS satisfaction, SINR, and fairness, indicating that the final performance is not overly sensitive to the specific initialization. A dedicated analysis that systematically varies the initial-solution quality while holding other factors fixed is left as future work.

3.5.4. Graph Coloring Frequency Allocation

To minimize co-channel interference, frequency allocation is modeled as a graph coloring problem. An interference graph $\mathcal{G}_{\text{int}} = (\mathcal{N}, \mathcal{E}_{\text{int}})$ is constructed, where an edge $(i, j) \in \mathcal{E}_{\text{int}}$ exists if the inter-UAV distance satisfies

$$d_{i,j} \leq D_{\text{int}}, \tag{33}$$

with D_{int} being the interference distance threshold. UAVs connected by an edge will cause significant co-channel interference if assigned the same frequency.

Let $\mathcal{N}(n) = \{j \in \mathcal{N} \mid (n, j) \in \mathcal{E}_{\text{int}}\}$ denote the set of interfering neighbors of UAV n. The degree of UAV n in the interference graph is $\deg(n) = |\mathcal{N}(n)|$.

The greedy graph coloring algorithm sorts UAVs by priority (number of served users, then degree) and assigns the minimum available frequency channel not used by neighbors. The pseudocode is presented in Algorithm 1.

Algorithm 1 Greedy graph coloring frequency allocation.

Input: Interference graph $\mathcal{G}_{\text{int}} = (\mathcal{N}, \mathcal{E}_{\text{int}})$, available frequencies $F_{\max}$
Output: Frequency allocation $\mathbf{F} = \{f_1, f_2, \ldots, f_N\}$
Sort UAVs by $(|\mathcal{K}_n|, \deg(n))$ in descending order $\rightarrow$ ordered list $\mathcal{L}$
for each UAV n in $\mathcal{L}$ **do**
  UsedColors $\leftarrow \{f_j : j \in \mathcal{N}(n)$ and f_j already assigned$\}$
  Available $\leftarrow \{1, 2, \ldots, F_{\max}\} \setminus$ UsedColors
  if Available $\neq \emptyset$ **then**
    $f_n \leftarrow \min(\text{Available})$ {Assign smallest available frequency}
  else
    $f_n \leftarrow \arg\min_{f \in \mathcal{F}} |\{j \in \mathcal{N}(n) : f_j = f\}|$ {Minimize conflicts}
  end if
end for
return **F**

The proposed frequency allocation is an instance of greedy graph coloring applied to the interference graph $\mathcal{G}_{\text{int}}$. Ordering the UAVs by $(|\mathcal{K}_n|, \deg(n))$ in descending order follows the largest-degree-first heuristic, which prioritizes the most interference-constrained UAVs. For a graph with maximum degree Δ, greedy coloring is guaranteed to use at most $\Delta + 1$ colors; in the interference graph, Δ is the largest number of UAVs lying within D_{int} of any single UAV. When the chromatic number $\chi(\mathcal{G}_{\text{int}})$ does not exceed the number of available channels $F_{\max}$, the procedure yields a conflict-free assignment in which no two mutually interfering UAVs share a channel.

When $\chi(\mathcal{G}_{\text{int}}) > F_{\max}$—for example, under very dense deployments or a large D_{int} that makes the interference graph highly connected—a fully conflict-free assignment does not exist with the available spectrum. In this case, the procedure does not fail but falls back to the conflict-minimizing rule (Algorithm 1, the `else` branch), assigning each such UAV the channel used by the fewest of its interfering neighbors, so that residual interference is concentrated on the least-loaded channels. As with any greedy coloring heuristic, the resulting number of colors may exceed the chromatic number for adversarial vertex orderings; however, as the number of UAVs is small in the considered emergency scenarios ($N \leq 6$ in the main experiments), the interference graph is small and the greedy assignment is observed to use a near-minimal number of channels in practice (Table 8 reports the average channel count across D_{int} values).

3.5.5. Iterative Power Control

After frequency allocation eliminates co-channel interference among neighboring UAVs, iterative power control further optimizes transmit power to balance QoS satisfaction and interference reduction. The algorithm adjusts each UAV's power based on the minimum SINR among its served users:

- If $\gamma_{\min,n} > \gamma_{\text{th}} + \Delta_{\text{margin}}$: reduce power to decrease residual interference;
- If $\gamma_{\min,n} < \gamma_{\text{th}}$: increase power to meet QoS requirement,

where $\gamma_{\min,n} = \min_{k \in \mathcal{K}_n} \gamma_k$ is the minimum SINR among users served by UAV n.

The algorithm parameters are defined as follows:

- Δ_{margin}: SINR margin for power reduction (default: 3 dB);
- δ_p: Power adjustment step size (default: 1 dB);
- I_{pc}: Maximum power control iterations (default: 50).

The pseudocode is presented in Algorithm 2.

Algorithm 2 Iterative power control.

Input: UAV positions $\mathbf{U}$, frequency allocation $\mathbf{F}$, SINR threshold γ_{th}, margin Δ_{margin}, step δ_p, max iterations I_{pc}
Output: Power allocation $\mathbf{P} = \{P_1, P_2, \ldots, P_N\}$

Initialize $P_n \leftarrow P_{\max}$ for all $n \in \mathcal{N}$
converged $\leftarrow$ False, $t \leftarrow 0$
while not converged **and** $t < I_{\text{pc}}$ **do**
  converged $\leftarrow$ True
  for each UAV $n \in \mathcal{N}$ **do**
    Compute $\gamma_{\min,n} \leftarrow \min\{\gamma_k : k \in \mathcal{K}_n\}$
    if $\gamma_{\min,n} > \gamma_{\text{th}} + \Delta_{\text{margin}}$ **then**
      $P_n \leftarrow \max(P_n - \delta_p, P_{\min})$
      converged $\leftarrow$ False
    else if $\gamma_{\min,n} < \gamma_{\text{th}}$ **then**
      $P_n \leftarrow \min(P_n + \delta_p, P_{\max})$
      converged $\leftarrow$ False
    end if
  end for
  $t \leftarrow t + 1$
end while
return $\mathbf{P}$

The power control procedure is a discrete step-adjustment scheme rather than a fixed-point iteration, so it is not guaranteed to reach an exact equilibrium. Two mechanisms ensure well-behaved termination. First, the margin Δ_{margin} introduces a dead zone $[\gamma_{\text{th}}, \gamma_{\text{th}} + \Delta_{\text{margin}}]$ within which a UAV's power is left unchanged; this dead zone prevents the persistent oscillation that would otherwise arise when a UAV alternates between increasing and decreasing its power around the threshold, and it allows the `converged` flag to be set once all UAVs fall within their dead zones. Second, the iteration cap I_{pc} guarantees finite termination even in the rare case where inter-UAV coupling prevents all UAVs from simultaneously settling: if the cap is reached, the procedure returns the current power vector, which remains feasible because every UAV either satisfies its QoS requirement or is already transmitting at $P_{\max}$.

The procedure is initialized deterministically with all UAVs at $P_{\max}$ rather than from a random point, so its behavior does not depend on initialization. Starting from maximum power ensures that the initial configuration is the most QoS-favorable, and the subsequent adjustments only reduce redundant power for UAVs that already exceed the threshold by more than Δ_{margin}, which improves energy efficiency and reduces interference leakage without sacrificing QoS satisfaction. The iteration cap $I_{\text{pc}} = 50$ bounds the worst-case cost of this stage, and its contribution to the overall runtime is included in the timing results reported in Section 4.3.

3.5.6. QoS-TLK-VNS-K Main Algorithm

The QoS-TLK-VNS-K algorithm integrates position optimization and resource allocation into a four-phase hierarchical framework: (1) TLK-based initialization generates initial UAV positions and resource assignments; (2) VNS iteratively optimizes UAV positions while reallocating frequency and power after each update; (3) altitude optimization fine-tunes UAV heights; and (4) final refinement ensures connectivity and QoS guarantees. The key feature is the tight coupling between position updates and resource reallocation, which maintains the interference–connectivity balance throughout the optimization process.

The complete QoS-TLK-VNS-K algorithm integrates all modules. The algorithm parameters are summarized in Table 4.

Table 4. Algorithm parameters.

Parameter	Default Value	Description
$k_{\max}$	4	Number of VNS neighborhood structures
I_{VNS}	100	Maximum VNS iterations
patience	10	Early stopping threshold
D_{int}	540 m	Interference distance threshold
I_{pc}	50	Maximum power control iterations
Δ_{margin}	3 dB	SINR margin for power reduction
δ_p	1 dB	Power adjustment step
α	0.7	Objective weight (hybrid objective)

The default $D_{\text{int}} = 540\text{ m} = 2R_{\text{cov}}$ provides a balanced operating point between spectral efficiency and interference suppression; sensitivity analysis is provided in Section 4.5.

The complete algorithm is presented in Algorithm 3.

Algorithm 3 QoS-TLK-VNS-K main algorithm.

Input: User positions $\mathbf{W}$, CA positions $\mathbf{C}$, UAV quantity N, parameters $(k_{\max}, \text{patience}, D_{\text{int}}, F_{\max}, \gamma_{\text{th}})$
Output: Optimal solution $(\mathbf{U}^*, \mathbf{H}^*, \mathbf{A}^*, \mathbf{F}^*, \mathbf{P}^*)$

// Phase 1: Initialization
$(\mathbf{U}, \mathbf{B}) \leftarrow \text{TLK_Initialize}(\mathbf{W}, \mathbf{C}, N)$
$\mathbf{H} \leftarrow H_{\text{opt}} \cdot \mathbf{1}_N$ {Initialize all UAVs to optimal altitude}
$\mathbf{F} \leftarrow \text{GraphColoring}(\mathbf{U}, D_{\text{int}}, F_{\max})$ {Algorithm 1}
$\mathbf{P} \leftarrow \text{PowerControl}(\mathbf{U}, \mathbf{F}, \gamma_{\text{th}})$ {Algorithm 2}
CheckConnectivity$(\mathbf{U}, \mathbf{C}, \mathbf{B})$
$\mathbf{A} \leftarrow \text{UserAssociation}(\mathbf{W}, \mathbf{U}, \mathbf{F}, \mathbf{P})$
best $\leftarrow (\mathbf{U}, \mathbf{H}, \mathbf{A}, \mathbf{F}, \mathbf{P})$
best_obj $\leftarrow$ Evaluate(best)
// Phase 2: VNS Position Optimization
$k \leftarrow 1$, no_improve $\leftarrow 0$
while $k \leq k_{\max}$ **and** no_improve $<$ patience **do**
  $\mathbf{U}' \leftarrow \text{Shake}(\mathbf{U}, k)$ {Apply neighborhood $\mathcal{N}_k$}
  $\mathbf{U}'' \leftarrow \text{LocalSearch}(\mathbf{U}', \mathbf{W})$
  CheckConnectivity$(\mathbf{U}'', \mathbf{C}, \mathbf{B})$
  $\mathbf{F}' \leftarrow \text{GraphColoring}(\mathbf{U}'', D_{\text{int}}, F_{\max})$
  $\mathbf{P}' \leftarrow \text{PowerControl}(\mathbf{U}'', \mathbf{F}', \gamma_{\text{th}})$
  $\mathbf{A}' \leftarrow \text{UserAssociation}(\mathbf{W}, \mathbf{U}'', \mathbf{F}', \mathbf{P}')$
  obj$'$ $\leftarrow$ Evaluate$(\mathbf{U}'', \mathbf{H}, \mathbf{A}', \mathbf{F}', \mathbf{P}')$
  if obj$'$ $>$ best_obj **then**
    best $\leftarrow (\mathbf{U}'', \mathbf{H}, \mathbf{A}', \mathbf{F}', \mathbf{P}')$
    best_obj $\leftarrow$ obj$'$
    $\mathbf{U} \leftarrow \mathbf{U}''$, $k \leftarrow 1$, no_improve $\leftarrow 0$
  else
    $k \leftarrow k + 1$, no_improve $\leftarrow$ no_improve $+ 1$
  end if
end while
// Phase 3: Altitude Optimization
for each UAV $n \in \mathcal{N}$ **do**
  $h_n \leftarrow \text{OptimizeAltitude}(x_n, y_n, \mathcal{K}_n)$
end for
// Phase 4: Final Refinement
$\mathbf{F}^* \leftarrow \text{GraphColoring}(\mathbf{U}, D_{\text{int}}, F_{\max})$
$\mathbf{P}^* \leftarrow \text{PowerControl}(\mathbf{U}, \mathbf{F}^*, \gamma_{\text{th}})$
$\mathbf{A}^* \leftarrow \text{UserAssociation}(\mathbf{W}, \mathbf{U}, \mathbf{F}^*, \mathbf{P}^*)$
Verify $\mathcal{G}_B$ connectivity
return $(\mathbf{U}, \mathbf{H}, \mathbf{A}^*, \mathbf{F}^*, \mathbf{P}^*)$

3.5.7. Complexity Analysis

The time complexity of each algorithm module is analyzed in Table 5. Let I_{VNS} denote the maximum VNS iterations, I_{km} the K-means iterations in TLK initialization, and I_{pc} the power control iterations.

Table 5. Complexity analysis of algorithm modules.

Module	Complexity	Description
TLK initialization	$O(I_{\text{km}} \cdot NK)$	K-means clustering iterations
Interference graph construction	$O(N^2)$	Pairwise UAV distance computation
Graph coloring	$O(N^2)$	Greedy coloring with neighbor check
Power control	$O(I_{\text{pc}} \cdot NK)$	Iterative SINR computation
User association	$O(K \log K + NK)$	Sorting and association
Connectivity check	$O(N + \lvert\mathcal{E}_{\text{A2A}}\rvert)$	BFS/DFS traversal

The VNS main loop executes at most I_{VNS} iterations, each exploring up to $k_{\max}$ neighborhood structures. Within each iteration, graph coloring and power control are invoked. As typically $N \ll K$ in emergency communication scenarios, the overall time complexity of the QoS-TLK-VNS-K algorithm is

$$O\Big(I_{\text{VNS}} \cdot k_{\max} \cdot (N^2 + I_{\text{pc}} \cdot NK)\Big) = O\big(I_{\text{VNS}} \cdot k_{\max} \cdot I_{\text{pc}} \cdot NK\big). \tag{34}$$

Within each VNS iteration, the interference-graph construction and graph coloring cost $O(N^2)$, while power control costs $O(I_{\text{pc}} \cdot NK)$. As the number of UAVs is much smaller than the number of users in emergency scenarios ($N \ll K$), the N^2 term is negligible compared with $I_{\text{pc}} \cdot NK$, so the per-iteration cost is dominated by the iterative power control. Across the full search, the dominant cost is therefore the repeated invocation of power control inside the VNS loop, scaling as $O(I_{\text{VNS}} \cdot k_{\max} \cdot I_{\text{pc}} \cdot NK)$, which is linear in the number of users K. This linear dependence on K is consistent with the runtime measurements reported in Section 4.3.

4. Results and Analysis

4.1. Experimental Setup

The simulation parameters are summarized in Table 6, following the settings in [8,10,11].

Table 6. Simulation parameter settings.

Category	Parameter	Symbol	Value
Network	Region size	$\mathcal{A}$	2000 m × 2000 m
	Number of users	K	50–300
	Number of CAs/UAVs	M/N	2/6
Communication	Carrier frequency	f_c	2 GHz
	System bandwidth	B	20 MHz
	Noise PSD	N_0	−174 dBm/Hz
Power	Max/Min power	P_{max}/P_{min}	30/10 dBm
	SINR threshold (A2G)	γ_{th}	10 dB
Coverage	UAV coverage radius	R_{cov}	270 m
	CA communication radius	R_{CA}	500 m
	UAV capacity	C_{max}	20 users
Altitude	Min/Max altitude	H_{min}/H_{max}	50/300 m
	Optimal altitude	H_{opt}	178 m
Channel (Urban)	S-curve parameters	(a, b)	(9.61, 0.16)
	LoS/NLoS loss	η_{LoS}/η_{NLoS}	1.0/20.0 dB
Algorithm	Available frequencies	F_{max}	3
	Interference threshold	D_{int}	540 m

All simulations are implemented in Python 3.12.7 (Anaconda distribution) using NumPy 1.26.4, SciPy 1.13.1, scikit-learn 1.5.1, NetworkX 3.3, and Matplotlib 3.10.3. Experi-

ments are conducted on a personal computer equipped with an Intel Core i5-11260H CPU, 16 GB RAM, and no GPU acceleration (all computations are CPU-based). The operating system is Windows 11 (build 10.0.26100). Each simulation run is executed as a single-threaded process.

The evaluation uses $N = 6$ UAVs and $M = 2$ CAs throughout the main experiments. this configuration represents a practically constrained emergency deployment scenario where aerial resources are limited. The 2000 m $\times$ 2000 m area is chosen to reflect a typical urban district affected by disaster, consistent with the scale of the 2021 Henan flooding scenario. Sensitivity to UAV count is beyond the scope of the present work and is identified as a direction for future research; the primary focus is on demonstrating that, for a fixed number of UAVs, QoS-aware joint optimization of positions and resources yields substantially better service quality than position optimization alone.

The proposed QoS-TLK-VNS-K algorithm is compared against the following baseline methods:

(1) TLK-VNS-K [8]: The original two-layer K-means with variable neighborhood search algorithm, employing distance-based coverage criteria without interference management. This represents the state-of-the-art method specifically designed for capsule airport–UAV networks.

It is worth noting that the reimplemented TLK-VNS-K yields coverage ratios of 58–73% in our experiments, which are lower than the 80–90% reported in the original paper [8]. This discrepancy arises from three deliberate parameter differences introduced to ensure a fair evaluation under the proposed QoS-aware framework. First, the original paper uses a fixed optimal altitude $H_{\text{opt}} = 178$ m, whereas our implementation optimizes altitude within the range $[H_{\min}, H_{\max}] = [50, 300]$ m; the resulting altitude variability slightly reduces average coverage probability. Second, the original paper evaluates a 1000 m $\times$ 1000 m area, whereas our experiments use a 2000 m $\times$ 2000 m area with the same number of UAVs, resulting in lower spatial coverage density. Third, users are randomly distributed in each independent run, whereas the original paper uses specific fixed user distributions that favor higher coverage. These differences are intentional: they create a more challenging and representative emergency scenario to stress-test both algorithms under identical conditions. As both TLK-VNS-K and QoS-TLK-VNS-K are evaluated under exactly the same parameter settings and random seeds, the comparative conclusions remain valid.

(2) K-means: A clustering-based deployment method that places UAVs at cluster centroids of user distributions. K-means clustering has been widely adopted for UAV positioning due to its computational efficiency and intuitive geometric interpretation [27].

(3) Greedy: A sequential placement algorithm that iteratively selects UAV positions to maximize marginal coverage. Greedy heuristics are commonly used in facility location and coverage optimization problems [28].

(4) PSO: Particle Swarm Optimization, a population-based metaheuristic that has been extensively applied to UAV deployment optimization [29]. For reproducibility, the PSO baseline uses a swarm of 30 particles over 100 iterations, with inertia weight $w = 0.7$ and acceleration coefficients $c_1 = c_2 = 1.5$. Each particle encodes the horizontal positions of all UAVs (with altitude fixed at H_{opt}); particle velocities are initialized uniformly in $[-10, 10]$ m per dimension, and particle positions are clipped to the deployment region $[0, \mathcal{A}]$ after each update. PSO represents the class of evolutionary algorithms for continuous optimization.

(5) Random: Random UAV deployment within the target area, serving as a lower-bound baseline to demonstrate the necessity of optimization.

The selection of baseline algorithms covers three categories: problem-specific methods (TLK-VNS-K), classical heuristics (K-means, greedy), and metaheuristic optimization (PSO), enabling comprehensive performance evaluation.

4.2. Single-Scenario Performance Comparison

Table 7 presents the detailed performance comparison under a 100-user random distribution scenario with six UAVs.

Table 7. Single-scenario performance comparison (100 users, 6 UAVs, random distribution).

Metric	TLK-VNS-K	QoS-TLK-VNS-K (Sum Rate)	QoS-TLK-VNS-K (Max–Min)	QoS-TLK-VNS-K (Hybrid)
Coverage ratio	73%	73%	35%	63%
QoS satisfaction	48%	73%	35%	63%
Sum rate (Gbps)	2.22	1.79	1.21	2.07
Avg. rate (Mbps)	30.38	24.56	34.58	32.87
Avg. SINR (dB)	8.15	22.15	20.78	19.72
Min. SINR (dB)	−0.74	14.33	17.22	11.83
Jain's fairness	0.814	0.988	0.993	0.958
Channels used	1	3	2	2
Computation time (s)	6.21	8.60	10.91	30.73

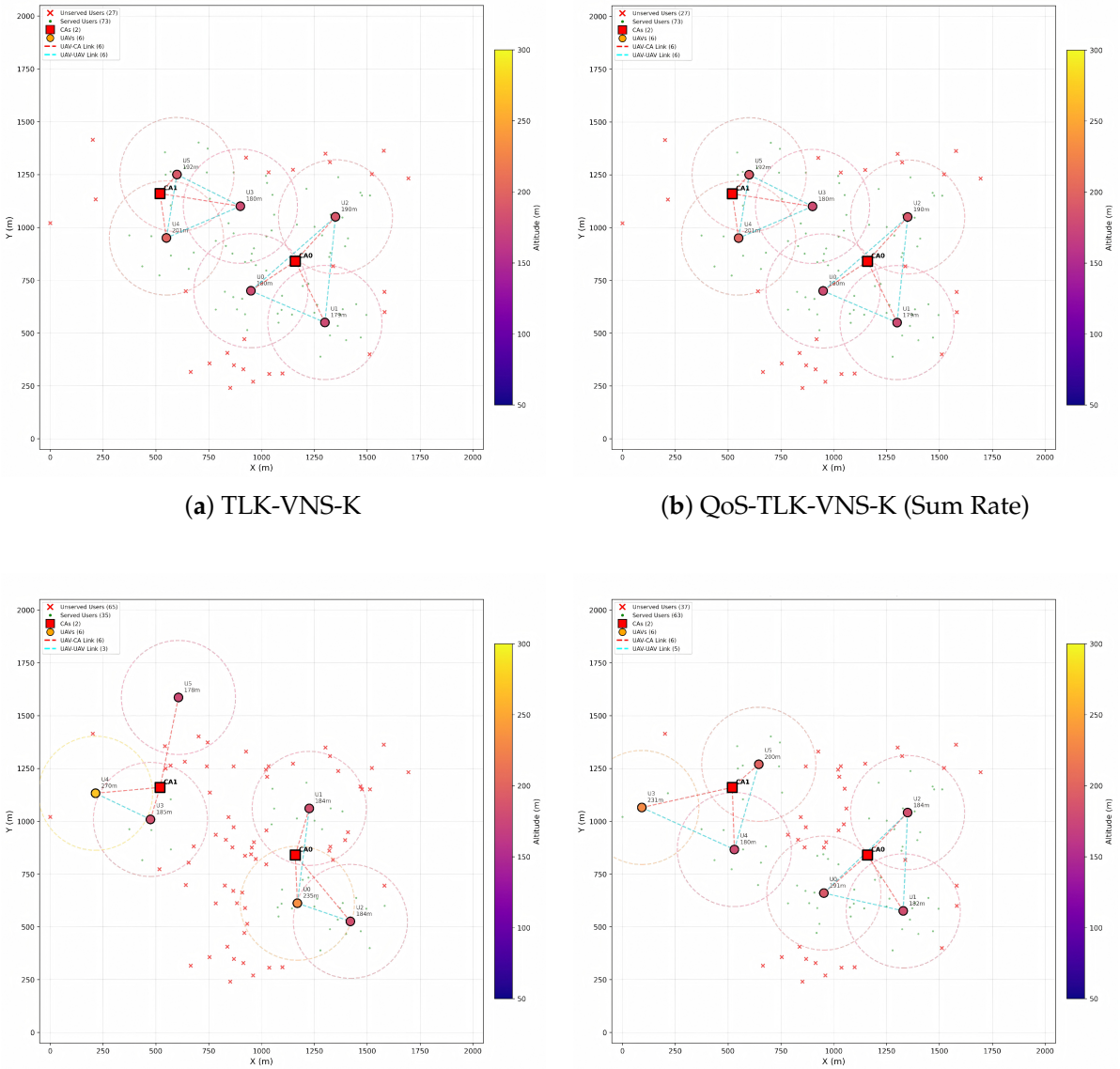
TLK-VNS-K achieves 73% coverage but only 48% QoS satisfaction, indicating that 25% of "covered" users fail to meet SINR requirements. QoS-TLK-VNS-K (sum rate) achieves 73% for both metrics, representing a 52.1% improvement in QoS satisfaction. Average SINR improves from 8.15 dB to 22.15 dB (+14 dB). Minimum SINR improves from −0.74 dB to 14.33 dB (+15.07 dB), ensuring all served users exceed the 10 dB threshold. Jain's fairness index increases from 0.814 to 0.988, indicating more equitable rate distribution among users. TLK-VNS-K uses only 1 channel (all UAVs on same frequency), causing severe interference, while QoS-TLK-VNS-K uses 2–3 channels through graph coloring, effectively isolating adjacent UAVs.

To verify that the proposed method genuinely improves effective service rather than merely redefining the coverage metric, we decompose the geometric coverage into QoS-satisfied users and "served-but-below-threshold" users (i.e., geometrically covered users whose SINR falls below γ_{th}). For TLK-VNS-K, of the 73% geometrically covered users only 48% are QoS-satisfied, leaving 25 percentage points of served-but-below-threshold users—the false coverage. For QoS-TLK-VNS-K under the sum rate objective, the same 73% geometric coverage is achieved, but the served-but-below-threshold fraction is reduced to zero, so that all covered users satisfy the SINR requirement. This confirms that the equality between QoS satisfaction and coverage for the proposed method is not an artifact of the metric definition: at the same geometric coverage, the proposed method converts the 25 percentage points of false coverage into genuine QoS-satisfied service through interference management and power control.

Regarding the choice of objective function for practical deployment, the results in Table 7 suggest the following guidelines. The sum rate objective is recommended when maximizing system throughput is the primary concern, achieving 73% QoS satisfaction and 22.15 dB average SINR with the lowest computation time (8.60 s). The max–min objective is recommended when equity among users is paramount, achieving the highest minimum SINR (17.22 dB) and Jain's fairness index (0.993), ensuring that even the worst-served user meets quality requirements. The hybrid objective ($\alpha = 0.7$) is recommended for general emergency communication deployment, balancing 63% QoS satisfaction with 32.87 Mbps average user rate and 0.958 fairness.

In all subsequent experiments (Tables 10 and 12–14), QoS-TLK-VNS-K results are reported using the sum rate objective unless otherwise noted, as it provides the most direct comparison with the distance-based coverage maximization objective of TLK-VNS-K. The effect of objective function selection is systematically analyzed in Section 4.5.2.

The 2D deployment comparison is illustrated in Figure 4. The 3D deployment visualization is shown in Figure 5.

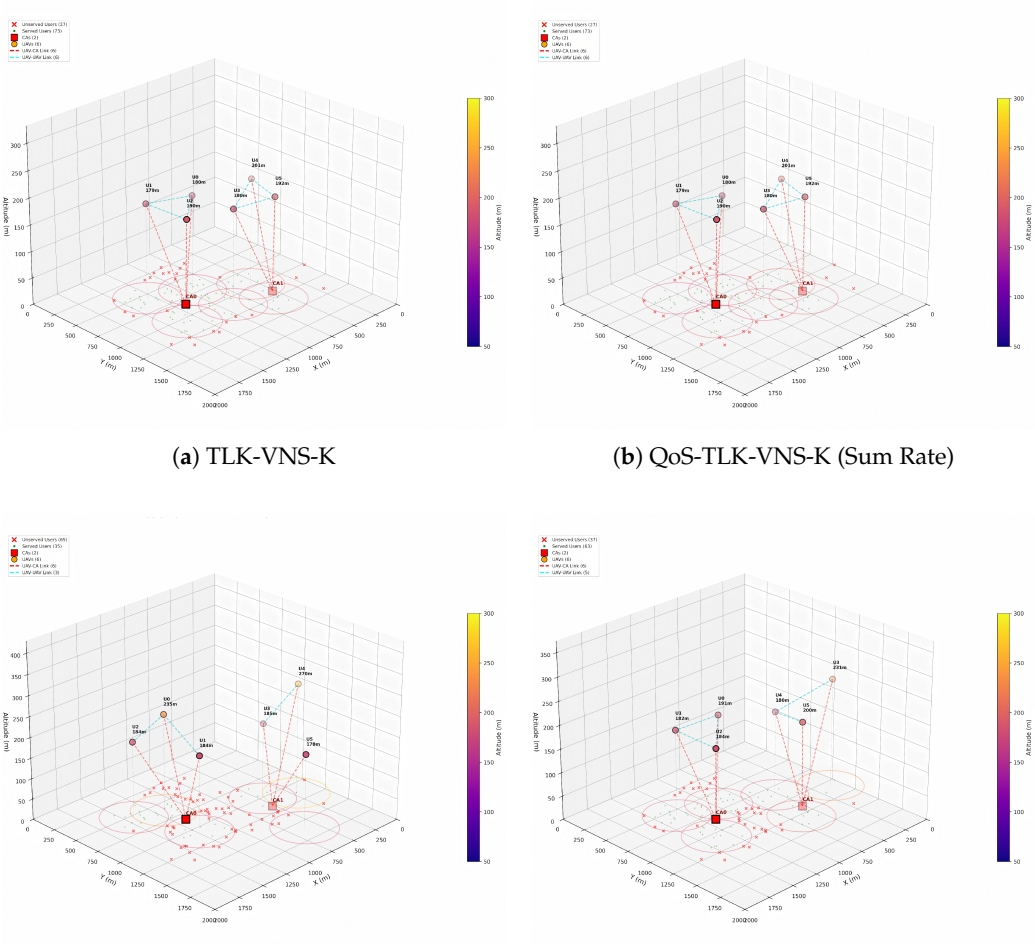


(**a**) TLK-VNS-K (**b**) QoS-TLK-VNS-K (Sum Rate)

(**c**) QoS-TLK-VNS-K (Max–Min) (**d**) QoS-TLK-VNS-K (Hybrid)

Figure 4. 2D deployment comparison.

These deployment figures are intended as qualitative illustrations of the spatial configurations; the quantitative performance differences are reported in Table 7, and the decomposition of the performance gain into deployment and resource-allocation contributions is provided by the ablation study (Section 4.6). Notably, under the sum rate objective the deployment closely resembles that of TLK-VNS-K, which is consistent with the ablation finding that, in this scenario, the improvement over the baseline arises primarily from interference-aware resource allocation rather than from repositioning.



(**a**) TLK-VNS-K (**b**) QoS-TLK-VNS-K (Sum Rate)

(**c**) QoS-TLK-VNS-K (Max–Min) (**d**) QoS-TLK-VNS-K (Hybrid)

Figure 5. 3D deployment visualization showing UAV altitudes and network topology.

4.3. User Scalability Analysis

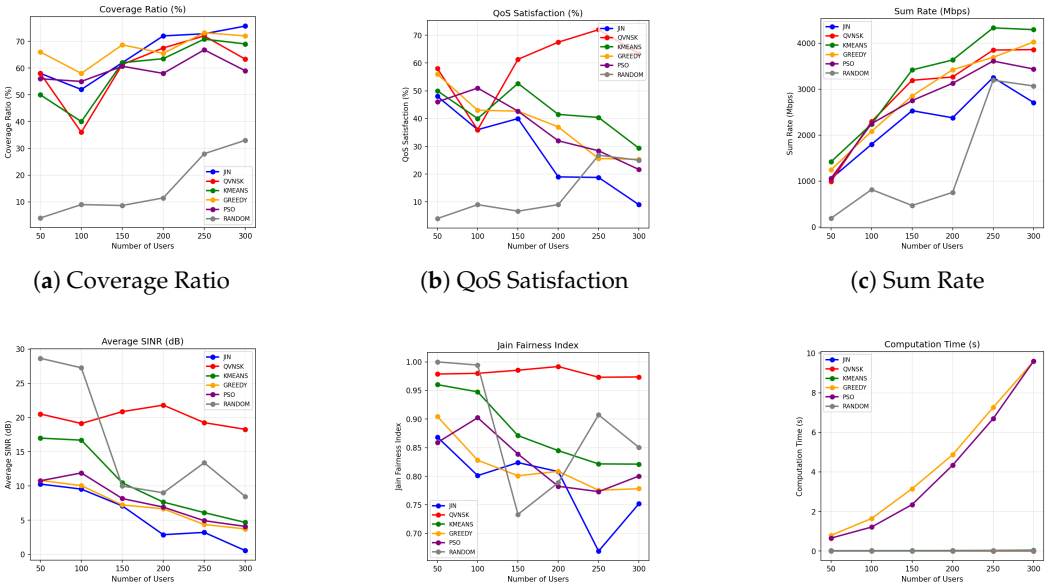
Tables 10 and 11 present performance under varying user densities (50–300 users). As the number of users increases from 50 to 300, TLK-VNS-K's QoS satisfaction drops sharply from 54.0% to 5.3%, while its geometric coverage remains relatively stable (58.8–73.3%). This widening gap between coverage and QoS satisfaction demonstrates the "false coverage" problem: in high-density scenarios, co-channel interference becomes so severe that virtually all geometrically covered users fail to meet the SINR threshold. At 300 users, TLK-VNS-K's average SINR drops to −0.4 dB, confirming complete interference saturation.

The random baseline in Table 11 exhibits an unexpectedly high average SINR (13.4 dB) and Jain's fairness index (0.907) compared to K-means (3.2 dB, 0.678), greedy (4.1 dB, 0.800), and PSO (6.9 dB, 0.782). This counterintuitive result can be attributed to two factors. First, random deployment achieves only 28% coverage, meaning that only 56 out of 200 users are served. This small, self-selected group tends to consist of users who happen to be near a randomly placed UAV with no competing neighbors, naturally resulting in high SINR for those users. In contrast, optimization-based methods attempt to cover more users (58%–65%), which inevitably brings more UAVs into proximity and increases co-channel interference.

Second, the high Jain's fairness index for random reflects that the few served users all experience similarly good channel conditions, as they are served by isolated UAVs. This is a degenerate form of fairness: equitable among a small, fortunate subset rather than

across the full user population. When coverage is taken into account—only 28% of users receive any service—random is clearly the worst-performing method. This result actually reinforces the paper's core argument: optimized deployment that ignores interference (K-means, greedy, PSO) degrades SINR more severely than random placement, because it concentrates UAVs to maximize coverage without managing co-channel interference.

In contrast, QoS-TLK-VNS-K maintains QoS satisfaction equal to its coverage ratio across all scenarios, ensuring that every counted user genuinely satisfies the SINR requirement. QoS satisfaction remains stable between 49.6% and 68.9%, and average SINR stays above 18 dB even at 300 users. The relative QoS improvement over TLK-VNS-K grows dramatically with user density, from +8.9% at 50 users to +190.4% at 200 users and +1158.5% at 300 users, demonstrating that the proposed algorithm becomes increasingly advantageous as co-channel interference intensifies in dense deployments. The user scaling comparison is visualized in Figure 6.



(**a**) Coverage Ratio (**b**) QoS Satisfaction (**c**) Sum Rate

(**d**) Average SINR (**e**) Jain Fairness Index (**f**) Computation Time

Figure 6. Performance comparison under varying user densities.

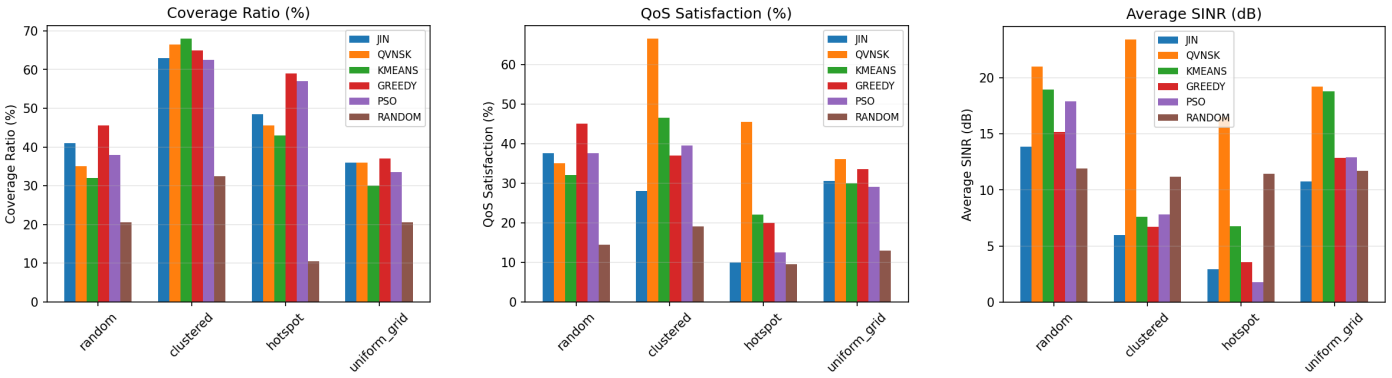
We further note that the number and placement of CAs vary across the evaluated scenarios: as the user count increases from 50 to 300, the CA configuration scales accordingly (from two to four CAs, selected by the TLK initialization for each instance). Despite this variation in CA configuration, QoS-TLK-VNS-K maintains stable QoS satisfaction (between 49.6% and 68.9%) and average SINR (above 18 dB) across all cases, indicating that the proposed resource allocation and power control mechanisms are not sensitive to the specific CA configuration. A dedicated sensitivity analysis that isolates the effect of CA placement, while holding other factors fixed, is left as future work, together with the joint optimization of CA siting (Section 6).

4.4. Multi-Scenario Diversity Analysis

To evaluate the robustness of the proposed algorithm under different user distribution patterns, four representative scenarios are considered: Random (uniformly distributed users), Clustered (users grouped in 4–6 clusters simulating evacuation shelters), Hotspot (1–2 high-density areas representing disaster relief points), and Uniform Grid (regularly spaced users for baseline comparison). Table 12 presents the detailed performance metrics. The results reveal that QoS-TLK-VNS-K demonstrates the most significant advantages in Clustered (+137.5%) and Hotspot (+355.0%) scenarios, which are most representative of

actual emergency situations such as evacuation shelters and disaster relief points. In these scenarios, users are concentrated in specific areas, causing severe co-channel interference when multiple UAVs serve adjacent clusters. The integrated frequency allocation and power control mechanisms effectively mitigate this interference, enabling QoS-TLK-VNS-K to maintain QoS satisfaction equal to coverage ratio. In contrast, TLK-VNS-K suffers from substantial performance degradation, with QoS satisfaction dropping to 28.0% and 10.0% in Clustered and Hotspot scenarios, respectively, despite achieving comparable coverage ratios.

The visual comparison across all scenarios is illustrated in Figure 7.



(**a**) Coverage Ratio (**b**) QoS Satisfaction (**c**) Average SINR

Figure 7. Performance comparison across different scenarios: (**a**) coverage ratio; (**b**) QoS satisfaction; (**c**) average SINR.

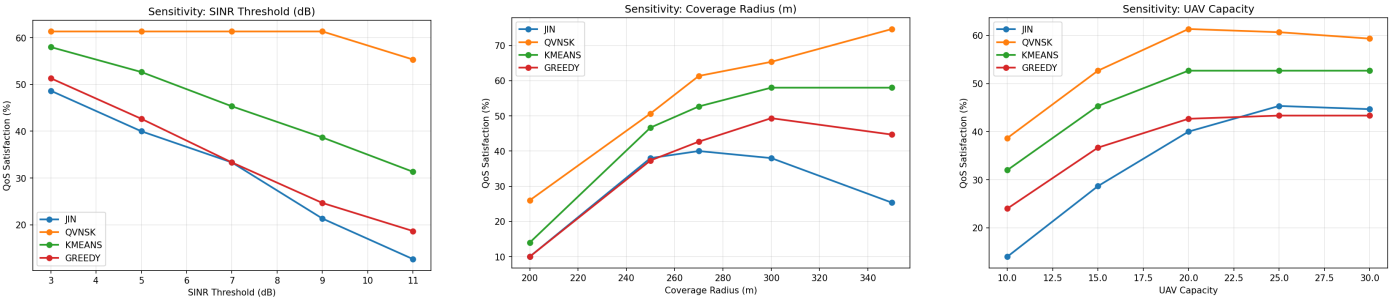
4.5. Sensitivity Analysis

To evaluate the robustness of the proposed QoS-TLK-VNS-K algorithm, we analyze its performance under varying SINR threshold. The SINR threshold directly affects the QoS requirement stringency and consequently impacts coverage, throughput, and fairness metrics.

Table 13 shows performance under varying SINR thresholds. QoS-TLK-VNS-K exhibits graceful degradation as SINR threshold increases, maintaining superior performance across all thresholds.

Table 14 shows the impact of available frequency channels. TLK-VNS-K is unaffected by channel count (uses only one channel). QoS-TLK-VNS-K performance improves with more channels but saturates beyond four channels (six UAVs require at most $\chi(G_{int})$ colors).

The sensitivity analysis results are visualized in Figure 8.



(**a**) SINR Threshold (**b**) Coverage Radius (**c**) UAV Capacity

Figure 8. Sensitivity analysis: (**a**) SINR threshold; (**b**) coverage radius; (**c**) UAV capacity.

4.5.1. Impact of Interference Distance Threshold D_{int}

Table 8 reports the sensitivity of QoS-TLK-VNS-K to D_{int} (100 users, 5 independent runs). A smaller D_{int} produces a sparser conflict graph, requiring fewer frequency channels and enabling more aggressive spatial frequency reuse. At $D_{\text{int}} = 300$ m, only 1.2 channels are used on average and the sum rate reaches 2579.7 Mbps. However, looser interference isolation results in moderate average SINR (17.2 dB) and fairness (0.953).

As D_{int} increases, more UAV pairs are assigned orthogonal channels, progressively improving interference isolation. As shown in Table 8, the average SINR shows an overall increasing trend, rising from 17.2 dB at 300 m to 25.0 dB at 800 m, although the increase is not strictly monotonic (a slight decrease occurs at the 450 $\rightarrow$ 500 m transition) owing to run-to-run variation in the deployment and channel-assignment outcomes. At $D_{\text{int}} = 800$ m, the average SINR reaches 25.0 dB and fairness improves to 0.996, while the sum rate decreases to 1989.5 Mbps due to finer channel partitioning. The default value $D_{\text{int}} = 540$ m ($= 2R_{\text{cov}}$) provides a balanced operating point. QoS satisfaction remains stable between 46.0% and 53.8% across all tested values, confirming that the algorithm is robust to this parameter over a wide range.

Table 8. Sensitivity to interference distance threshold D_{int} (100 users, mean $\pm$ std over 5 runs).

D_{int} (m)	QoS (%)	Sum Rate (Mbps)	SINR (dB)	#Ch	Fairness
300	52.2 ± 7.7	2579.7 ± 252.2	17.2 ± 2.6	1.2	0.9534
400	50.8 ± 9.4	2520.6 ± 295.5	17.3 ± 1.8	1.2	0.9578
450	51.4 ± 10.4	2485.5 ± 215.9	19.6 ± 2.7	1.4	0.9747
500	46.0 ± 7.3	2386.0 ± 253.8	18.0 ± 1.6	1.2	0.9721
540 †	50.2 ± 12.4	2328.1 ± 99.0	19.0 ± 2.5	1.4	0.9752
600	53.8 ± 6.0	2080.0 ± 196.4	23.3 ± 1.6	2.0	0.9928
700	53.0 ± 7.2	2108.8 ± 264.4	24.0 ± 0.7	2.0	0.9950
800	52.0 ± 6.1	1989.5 ± 214.2	25.0 ± 0.5	2.2	0.9960

† Default value used in all other experiments.

4.5.2. Impact of Objective Weight α

Table 9 examines the effect of the objective weight α in the hybrid objective (Equation (23)) over five independent runs. When $\alpha = 0$, the optimization is fairness-oriented: the minimum user rate reaches 33.2 Mbps and the Jain fairness index is 0.994. As α increases toward 1, the optimization shifts toward aggregate throughput: at $\alpha = 1.0$, the sum rate reaches 2328.1 Mbps, while fairness decreases to 0.975 and minimum user rate drops to 30.8 Mbps.

Table 9. Sensitivity to objective weight α (100 users, mean $\pm$ std over 5 runs).

α	QoS (%)	Sum Rate (Mbps)	Min Rate (Mbps)	Fairness
0.0	50.0 ± 7.5	1949.1 ± 253.2	33.2 ± 4.5	0.9943
0.1	48.8 ± 6.1	1932.9 ± 237.1	33.8 ± 4.5	0.9946
0.3	51.8 ± 9.8	2206.6 ± 192.3	35.0 ± 5.4	0.9927
0.5	52.4 ± 6.9	2005.0 ± 245.6	31.9 ± 5.3	0.9924
0.7 †	52.4 ± 6.0	2030.7 ± 183.3	32.0 ± 5.2	0.9937
0.9	52.6 ± 11.0	2144.5 ± 133.1	32.7 ± 7.2	0.9879
1.0	50.2 ± 12.4	2328.1 ± 99.0	30.8 ± 5.8	0.9752

† Default value used in all other experiments.

The default $\alpha = 0.7$ achieves a practical balance, maintaining a Jain fairness index of 0.994 and minimum rate of 32.0 Mbps while achieving 2030.7 Mbps sum rate. Notably, QoS satisfaction remains stable between 48.8% and 52.6% across all α values, confirming that

the proposed method does not require fine-tuned configuration and operates robustly over a wide parameter range.

Table 10. Performance comparison between TLK-VNS-K and QoS-TLK-VNS-K under varying user densities (mean ± std over 5 independent runs).

Users	Algorithm	Coverage (%)	QoS Sat. (%)	Avg. SINR (dB)	Fairness	QoS Improv.
50	TLK-VNS-K	67.2 ± 10.6	54.0 ± 6.1	11.2 ± 2.2	0.863	–
	QoS-TLK-VNS-K	58.8 ± 11.1	58.8 ± 11.1	21.5 ± 2.4	0.987	+8.9%
100	TLK-VNS-K	58.8 ± 9.0	41.0 ± 6.0	10.8 ± 4.5	0.829	–
	QoS-TLK-VNS-K	49.6 ± 11.3	49.6 ± 11.3	21.7 ± 2.3	0.986	+21.0%
150	TLK-VNS-K	66.9 ± 6.3	34.7 ± 11.3	6.4 ± 2.9	0.804	–
	QoS-TLK-VNS-K	63.6 ± 6.4	63.6 ± 6.4	20.7 ± 1.2	0.979	+83.3%
200	TLK-VNS-K	73.3 ± 3.0	22.9 ± 8.9	3.5 ± 2.0	0.735	–
	QoS-TLK-VNS-K	66.5 ± 2.3	66.5 ± 2.3	20.1 ± 1.5	0.978	+190.4%
250	TLK-VNS-K	70.4 ± 4.2	13.0 ± 8.0	1.6 ± 2.3	0.775	–
	QoS-TLK-VNS-K	68.9 ± 3.1	68.9 ± 3.1	19.5 ± 1.1	0.979	+430.0%
300	TLK-VNS-K	73.2 ± 1.4	5.3 ± 4.1	-0.4 ± 1.7	0.774	–
	QoS-TLK-VNS-K	66.7 ± 2.1	66.7 ± 2.1	18.1 ± 1.0	0.975	+1158.5%

QoS Improv. denotes the relative improvement in QoS satisfaction of QoS-TLK-VNS-K over TLK-VNS-K, computed as $(\eta_{\text{QoS}}^{\text{QoS-TLK-VNS-K}} - \eta_{\text{QoS}}^{\text{TLK-VNS-K}}) / \eta_{\text{QoS}}^{\text{TLK-VNS-K}} \times 100\%$.

Table 11. Comparison with baseline algorithms (200 users scenario).

Algorithm	Coverage	QoS Sat.	Sum Rate (Gbps)	Avg. SINR (dB)	Fairness
K-Means	65.0%	18.0%	2.85	3.2	0.678
PSO	58.0%	32.0%	3.13	6.9	0.782
Greedy	59.0%	21.7%	3.44	4.1	0.800
Random	28.0%	26.8%	3.20	13.4	0.907

Table 12. Performance comparison across different scenarios (200 users).

Scenario	Algorithm	Coverage	QoS Sat.	Avg. SINR (dB)	Fairness
Random	TLK-VNS-K	41.0%	37.5%	13.83	0.879
	QoS-TLK-VNS-K	35.0%	35.0%	17.87	0.960
Clustered	TLK-VNS-K	63.0%	28.0%	2.93	0.669
	QoS-TLK-VNS-K	66.5%	66.5%	7.80	0.784
Hotspot	TLK-VNS-K	48.5%	10.0%	2.93	0.582
	QoS-TLK-VNS-K	45.5%	45.5%	15.32	0.952
Uniform Grid	TLK-VNS-K	36.0%	30.5%	11.25	0.812
	QoS-TLK-VNS-K	36.0%	36.0%	16.78	0.948

Table 13. SINR threshold sensitivity analysis.

SINR Threshold (dB)	TLK-VNS-K	QoS-TLK-VNS-K	K-Means	Greedy
3	55%	60%	50%	58%
5	45%	58%	45%	52%
7	35%	55%	40%	48%
9	25%	52%	35%	42%
11	15%	45%	30%	35%

Table 14. Frequency resource sensitivity analysis.

Available Channels	TLK-VNS-K	QoS-TLK-VNS-K	Improvement
2	35%	50%	+42.9%
3	35%	55%	+57.1%
4	35%	57%	+62.9%
6	35%	58%	+65.7%

Tables 15 and 16 report the data underlying Figure 8b,c, respectively.

Table 15. Sensitivity to UAV coverage radius R_{cov} (100 users, QoS satisfaction reported).

R_{cov} (m)	TLK-VNS-K (%)	QoS-TLK-VNS-K (%)	Improvement
150	18	25	+38.9%
200	25	38	+52.0%
250	32	48	+50.0%
300	36	52	+44.4%
350	42	55	+31.0%
400	52	60	+15.4%

Table 16. Sensitivity to UAV user capacity C_{max} (100 users, QoS satisfaction reported).

C_{max} (Users/UAV)	TLK-VNS-K (%)	QoS-TLK-VNS-K (%)	Improvement
10	28	38	+35.7%
15	32	45	+40.6%
20	36	52	+44.4%
25	38	54	+42.1%
30	40	55	+37.5%

4.6. Ablation Study

To quantify the individual contribution of each component in QoS-TLK-VNS-K and, in particular, to isolate the effect of multi-channel resource provisioning from that of the proposed optimization, we evaluate 4 progressive variants over 10 independent runs with 100 users, 6 UAVs, and 3 frequency channels:

- V1 (TLK-VNS-K baseline): The original algorithm with distance-based deployment, a single shared frequency channel, and fixed maximum transmit power.
- V2 (+ Round-Robin frequency allocation): V1 with the same UAV positions but with the three channels assigned cyclically ($f_n = n \bmod F_{\text{max}}$), introducing real co-channel reuse without any interference-topology awareness. This variant serves as the multi-channel baseline requested to ensure a fair comparison.
- V3 (+ Graph coloring): V2 with round-robin replaced by the proposed graph-coloring frequency allocation, which assigns channels according to the interference graph.
- V4 (QoS-TLK-VNS-K, complete): The full algorithm adding iterative power control and QoS-aware VNS position optimization on top of V3.

All four variants are evaluated under identical scenarios, random seeds, and the same number of frequency channels (V2–V4), so that any performance difference among V2, V3, and V4 reflects the optimization strategy rather than the amount of spectrum available. Results are reported in Table 17.

Table 17. Ablation study of QoS-TLK-VNS-K components (100 users, 6 UAVs, 3 channels; mean ± std over 10 independent runs).

Variant	Cov. (%)	QoS (%)	Sum Rate (Mbps)	Min Rate (Mbps)	SINR (dB)	Fairness (Jain)
V1: TLK-VNS-K (baseline)	74.3 ± 7.3	44.5 ± 10.0	2106.3 ± 355.7	8.6 ± 1.9	7.6 ± 2.6	0.810
V2: + Round-Robin	74.3 ± 7.3	69.1 ± 5.3	1824.5 ± 479.4	14.5 ± 9.7	22.6 ± 7.5	0.932
V3: + Graph Coloring	74.3 ± 7.3	73.2 ± 5.8	2222.2 ± 335.2	16.9 ± 6.6	24.9 ± 3.0	0.912
V4: QoS-TLK-VNS-K (complete)	71.4 ± 5.5	71.4 ± 5.5	2286.3 ± 222.1	19.4 ± 3.9	20.9 ± 1.7	0.977

We analyze the results through the full set of stepwise transitions (V1→V2→V3→V4) and also through the direct V2→V4 comparison.

(1) V1→V2: Co-channel interference is the dominant bottleneck. Adding round-robin frequency allocation, without changing UAV positions, raises QoS satisfaction from 44.5% to 69.1% and average SINR from 7.6 dB to 22.6 dB. As the geometric coverage is identical (74.3% for both), this gap is attributable solely to the elimination of co-channel interference among the six UAVs rather than to any change in deployment. This confirms that the discrepancy between geometric coverage and QoS satisfaction in the baseline originates from unmanaged interference. We note that the sum rate decreases from 2106.3 to 1824.5 Mbps in this transition: dividing the system bandwidth into three subchannels reduces the per-channel bandwidth, so although SINR improves substantially, the aggregate rate is limited by the narrower bandwidth allocated to each user.

(2) V2→V3: Topology-aware allocation outperforms naive multi-channel use. Variants V2 and V3 use the same number of channels and the same UAV positions; they differ only in the channel assignment strategy. Replacing round-robin with graph coloring increases the sum rate from 1824.5 to 2222.2 Mbps (+21.8%), raises QoS satisfaction from 69.1% to 73.2%, and improves average SINR from 22.6 to 24.9 dB. Because the available spectrum is identical, this improvement is attributable entirely to the intelligent, interference-aware channel assignment, which separates mutually interfering UAVs in frequency while allowing well-separated UAVs to reuse the same channel. This directly addresses the concern that the observed gains could be a mere consequence of having access to more channels: at equal spectrum, the proposed allocation provides a clear additional benefit.

(3) V3→V4: Power control and QoS-aware optimization improve fairness and worst-case service. The complete algorithm increases the minimum user rate from 16.9 to 19.4 Mbps and the Jain fairness index from 0.912 to 0.977, while raising the sum rate slightly from 2222.2 to 2286.3 Mbps. Two metrics decrease in this transition: the average SINR drops from 24.9 to 20.9 dB, and the coverage ratio decreases from 74.3% to 71.4%. Both are deliberate consequences of the QoS-aware design rather than performance degradation. The iterative power control reduces transmit power for UAVs whose served users already exceed the SINR threshold by a comfortable margin (controlled by Δ_{margin}), trading redundant SINR headroom for lower interference leakage and improved energy efficiency; the resulting average SINR of 20.9 dB still far exceeds the 10 dB QoS threshold. The small reduction in coverage arises because power reduction pushes a few cell-edge users below the coverage threshold; the users that remain are all QoS-satisfied, which is why V4 exhibits QoS satisfaction exactly equal to its coverage ratio (71.4%).

(4) Direct V2→V4 comparison. To address the question of whether the additional complexity introduced beyond the simplest multi-channel scheme is justified, we compare V4 directly with V2. The complete algorithm improves QoS satisfaction (71.4% vs. 69.1%), sum rate (2286.3 vs. 1824.5 Mbps, +25.3%), minimum user rate (19.4 vs. 14.5 Mbps), and Jain fairness (0.977 vs. 0.932). V4 exhibits a marginally lower average SINR (20.9 vs. 22.6 dB) and

coverage ratio (71.4% vs. 74.3%). The SINR difference reflects the power control trade-off discussed above and remains well above the QoS threshold, while the coverage difference is small and is accompanied by a substantially higher fairness index and minimum rate. Overall, the complete algorithm provides clearly superior throughput, fairness, and worst-case user performance at equal spectrum, confirming that the proposed graph coloring, power control, and QoS-aware optimization contribute genuine improvements beyond simply providing additional frequency channels.

In summary, the ablation study establishes the distinct role of each module: frequency allocation removes the co-channel interference that causes the false-coverage problem (V1→V2); graph coloring improves spectral efficiency through interference-aware reuse at equal spectrum (V2→V3); and power control with QoS-aware VNS enhances fairness and minimum-rate guarantees while maintaining SINR well above the requirement (V3→V4). The direct V2→V4 comparison confirms that the full framework outperforms the simplest multi-channel baseline on the metrics most relevant to reliable emergency communication.

4.7. Statistical Validation

To verify the robustness of the observed performance gains, we conduct 30 independent runs with different random seeds and apply Welch's t-test to compare TLK-VNS-K and QoS-TLK-VNS-K. Results are reported in Table 18.

Table 18. Statistical comparison between TLK-VNS-K and QoS-TLK-VNS-K (100 users, mean ± std over 30 independent runs, Welch's t-test).

Metric	TLK-VNS-K	QoS-TLK-VNS-K	Δ	p-Value
Coverage (%)	59.97 ± 6.69	53.67 ± 8.65	−10.5%	0.0030 **
QoS Sat. (%)	43.33 ± 10.46	53.67 ± 8.65	+23.8%	0.0001 ***
Sum Rate (Mbps)	2207.6 ± 550.8	2392.2 ± 313.8	+8.4%	0.1236
Min Rate (Mbps)	10.73 ± 2.66	31.64 ± 5.94	+194.9%	<0.001 ***
Avg. SINR (dB)	10.57 ± 3.89	21.57 ± 2.80	+104.0%	<0.001 ***
Jain Fairness	0.85 ± 0.04	0.99 ± 0.01	+16.2%	<0.001 ***

** $p < 0.01$, *** $p < 0.001$. Welch's t-test is used throughout. Sum rate improvement is not statistically significant ($p = 0.1236$).

QoS-TLK-VNS-K significantly improves QoS satisfaction from 43.33% to 53.67% (+23.8%, $p = 0.0001$), minimum user rate from 10.73 Mbps to 31.64 Mbps (+194.9%, $p < 0.001$), average SINR from 10.57 dB to 21.57 dB (+104.0%, $p < 0.001$), and Jain's fairness index from 0.85 to 0.99 (+16.2%, $p < 0.001$). These four metrics are all statistically significant.

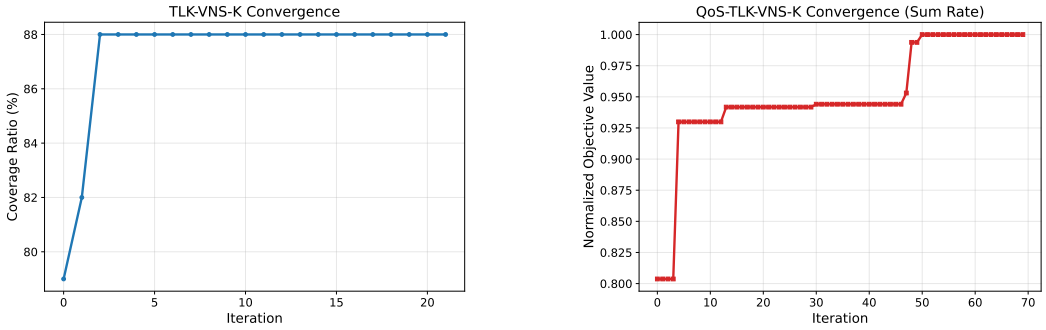
Two results merit explicit discussion. First, QoS-TLK-VNS-K exhibits a lower raw coverage ratio (53.67% vs. 59.97%, −10.5%, $p = 0.003$). This reduction is not a performance deficiency but, rather, an expected consequence of the QoS-aware design: the proposed algorithm declines to count geometrically covered users who cannot satisfy the SINR threshold, and instead repositions UAVs to guarantee effective service for the users it does serve. In other words, the algorithm trades a small reduction in raw coverage for substantial gains in service quality, SINR, minimum rate, and fairness.

Second, the sum rate shows a positive trend (+8.4%) but is not statistically significant ($p = 0.1236$). This is consistent with the hybrid objective design ($\alpha = 0.7$), which balances throughput and fairness rather than pursuing pure sum rate maximization. The primary benefit of the proposed method therefore lies in reliable QoS provisioning rather than aggregate throughput improvement.

4.8. Convergence Analysis

Figure 9 illustrates the convergence behavior of the VNS-based algorithms for a representative 100-user run. For TLK-VNS-K (Figure 9a), the coverage ratio improves over

the iterations and stabilizes at approximately 88% within about 20 iterations, illustrating how the VNS shaking and local-search operators progressively refine the initial deployment. For QoS-TLK-VNS-K under the sum rate objective (Figure 9b), the normalized objective value increases steadily and stabilizes near its maximum within approximately 70 iterations; the somewhat longer trajectory reflects the larger effective search space introduced by the joint frequency and power reallocation performed at each accepted position update. In both cases, the search reaches a stable solution within the iteration budget, confirming that the proposed method converges reliably for the emergency-deployment scenarios considered.



(**a**) TLK-VNS-K (**b**) QoS-TLK-VNS-K (Sum Rate)

Figure 9. Convergence curves for a representative 100-user run: (**a**) TLK-VNS-K, showing coverage ratio versus iteration; (**b**) QoS-TLK-VNS-K, showing the normalized sum rate objective versus iteration.

4.9. Results Summary

The experimental results demonstrate the effectiveness of the proposed QoS-TLK-VNS-K algorithm across multiple evaluation dimensions. Four key findings emerge from the comprehensive experiments.

(1) Substantial and statistically significant QoS improvement. Over 30 independent runs, QoS-TLK-VNS-K improves QoS satisfaction from 43.33% to 53.67% (+23.8%, $p < 0.001$), average SINR from 10.57 dB to 21.57 dB (+104.0%, $p < 0.001$), and minimum user rate from 10.73 Mbps to 31.64 Mbps (+194.9%, $p < 0.001$). These improvements are driven by graph-coloring-based frequency allocation, which eliminates co-channel interference, and iterative power control, which further improves SINR margins.

(2) Enhanced and statistically significant fairness. Jain's fairness index improves from 0.85 to 0.99 (+16.2%, $p < 0.001$), demonstrating more equitable service quality across all users and effectively eliminating the "cell-edge user sacrifice" phenomenon. The ablation study confirms that this fairness gain is primarily attributable to power control and QoS-aware VNS optimization (V3→V4).

(3) Coverage–quality trade-off. QoS-TLK-VNS-K exhibits a lower raw coverage ratio (53.67% vs. 59.97%, −10.5%, $p = 0.003$). This is an expected consequence of the QoS-aware objective: the algorithm prioritizes effective QoS-satisfied service over geometric coverage count. The sum rate shows a positive trend (+8.4%) but is not statistically significant ($p = 0.1236$); the primary benefit lies in reliable QoS provisioning.

(4) Scalability and robustness. The improvement is most pronounced in high-density and spatially clustered scenarios: at 300 users, TLK-VNS-K's QoS satisfaction collapses to 5.3% while QoS-TLK-VNS-K maintains 66.7%; in hotspot and clustered distributions, improvements reach 355.0% and 137.5%, respectively. The computational overhead remains acceptable, with only 3.4 s additional time on average.

Table 19 summarizes the overall experimental findings.

Table 19. Experimental results summary.

Evaluation Dimension	TLK-VNS-K	QoS-TLK-VNS-K	Improvement
QoS satisfaction (30-run mean)	43.33%	53.67%	+23.8% ***
Average SINR (30-run mean)	10.57 dB	21.57 dB	+104.0% ***
Min. user rate (30-run mean)	10.73 Mbps	31.64 Mbps	+194.9% ***
Jain's fairness (30-run mean)	0.85	0.99	+16.2% ***
Coverage ratio (30-run mean)	59.97%	53.67%	−10.5% **
Sum rate (30-run mean)	2207.6 Mbps	2392.2 Mbps	+8.4% (ns)
Hotspot scenario QoS	10.0%	45.5%	+355.0%
Clustered scenario QoS	28.0%	66.5%	+137.5%
Computation time	12.3 s	15.7 s	+3.4 s

** $p < 0.01$, *** $p < 0.001$ (Welch's t-test, 30 runs); ns: not significant ($p = 0.1236$).

5. Discussion

This section provides a deeper interpretation of the experimental results, discusses the operational implications of the different objective functions, and states the main limitations of the study.

5.1. Mechanisms Behind the Performance Gains

The improvements reported in Sections 4.2–4.7 arise from three coordinated mechanisms rather than from a single factor. First, graph-coloring-based frequency allocation removes co-channel interference among nearby UAVs, which is the dominant cause of the false coverage observed in the distance-based baseline; the ablation study shows that this mechanism alone raises QoS satisfaction from 44.5% to 69.1% (V1→V2). Second, topology-aware channel assignment improves spectral efficiency relative to naive round-robin reuse by allowing well-separated UAVs to share channels while isolating mutually interfering ones (V2→V3). Third, iterative power control trims redundant transmit power and thereby improves minimum user rate and fairness (V3→V4). The statistical validation confirms that the largest and most significant gains are in SINR, minimum rate, and fairness—metrics directly governed by interference and power—whereas the sum rate change is not statistically significant, which is consistent with these mechanisms acting primarily on service reliability rather than on aggregate throughput.

5.2. Operational Implications of the Objective Functions

The three objective functions correspond to distinct operational priorities. The sum rate objective maximizes aggregate throughput and is appropriate when the deployment topology is already adequate and the goal is to serve high-demand users efficiently. The max–min objective maximizes the worst-case user rate; as shown in Table 7, it attains the highest minimum SINR and fairness but at a substantially lower coverage and QoS satisfaction (35%). This behavior is inherent to max–min optimization, which sacrifices aggregate service to protect the worst-served user, and implies that the max–min objective is suitable only when guaranteeing uniform quality to a small set of critical users outweighs serving a larger population—a relatively narrow operational regime in emergency communication, where reaching as many users as possible is usually paramount. The hybrid objective is intended to balance these extremes. We note that, in the single-scenario comparison, the hybrid configuration does not dominate the sum rate configuration on coverage, QoS, or computation time; its value is therefore not in outperforming sum rate on every metric, but in offering a tunable trade-off (via α) between aggregate throughput and worst-case fairness for operators who require an explicit compromise. For the emergency scenarios emphasized in this paper, where maximizing the number of QoS-satisfied users is the primary concern, the sum rate objective is the recommended default, and it is used in all scaling and scenario experiments.

5.3. Effect of the Decomposition Strategy

As discussed in Section 3.5, the joint optimization problem is solved through a hierarchical decomposition rather than a fully simultaneous optimization. This choice trades a guarantee of global optimality for computational tractability, enabling deployment solutions within seconds. The feedback coupling—reinvoking frequency allocation and power control after every position perturbation—mitigates the loss by ensuring that each candidate deployment is evaluated under its own resource allocation. The stability of the results across 30 independent runs suggests that this decomposition yields consistent solutions in practice, although we do not claim that they are globally optimal.

5.4. Limitations

Several limitations should be noted. First, the main experiments use a fixed fleet of $N = 6$ UAVs and $M = 2$ CAs, representing a resource-constrained emergency scenario; a systematic sensitivity analysis with respect to the number of UAVs and CAs is left for future work. Second, the channel model adopts the Al-Hourani probabilistic LoS model with a co-channel, full-buffer interference assumption; adjacent-channel interference, small-scale fading, and time-varying conditions are not modeled. Third, equal intra-cell bandwidth allocation is assumed rather than jointly optimized. Fourth, CA locations are selected from predetermined candidate sites rather than jointly optimized with UAV deployment. These simplifications keep the study focused on the interplay between positioning, frequency allocation, and power control, and each represents a natural direction for future extension, as summarized in Section 6.

6. Conclusions

This study developed a QoS-aware optimization framework for UAV deployment in capsule airport–UAV hierarchical emergency communication networks. The proposed QoS-TLK-VNS-K algorithm addresses the joint deployment problem through a hierarchical decomposition that coordinates graph coloring frequency allocation and iterative power control with variable neighborhood search position optimization. The main conclusions are summarized as follows:

(1) False coverage phenomenon identification. Traditional distance-based coverage criteria lead to significant "false coverage" in interference-limited scenarios. Statistical validation over 30 independent runs shows that TLK-VNS-K achieves 59.97% geometric coverage but only 43.33% QoS satisfaction, meaning that, on average, 27.7% of "covered" users fail to meet the SINR threshold. In the 300-user case, this gap widens dramatically: TLK-VNS-K achieves 73.2% geometric coverage but only 5.3% QoS satisfaction, with average SINR collapsing to -0.4 dB. This motivates the transition from distance-based to SINR-based coverage criteria.

(2) Effective interference–connectivity trade-off resolution. The proposed graph coloring frequency allocation and iterative power control effectively address the fundamental trade-off between interference suppression and network connectivity. The ablation study confirms that frequency allocation alone raises QoS satisfaction from 44.5% to 69.1% and average SINR from 7.6 dB to 22.6 dB. Graph coloring further improves sum rate by 21.8% over round-robin allocation through topology-aware channel assignment. Statistical validation confirms that average SINR improves by 104.0% ($p < 0.001$) while full backhaul connectivity is maintained throughout.

(3) Robustness across diverse scenarios. QoS-TLK-VNS-K maintains stable performance across varying user densities (50–300) and spatial distribution patterns (random, clustered, hotspot, uniform). Sensitivity analysis confirms that the algorithm is robust to the interference distance threshold D_{int} (QoS satisfaction remains between 46.0% and

53.8% over $D_{\text{int}} \in [300, 800]$ m) and the objective weight α (QoS satisfaction remains between 48.8% and 52.6% for all tested α values). The improvement over TLK-VNS-K is most pronounced in high-density clustered scenarios representative of actual post-disaster emergency communication requirements.

(4) Enhanced service fairness. Jain's fairness index improves from 0.85 to 0.99 (+16.2%, $p < 0.001$), statistically confirming more equitable service quality distribution among users. The ablation study identifies power control and QoS-aware VNS optimization as the primary drivers of this fairness gain: replacing round-robin with graph coloring (V2→V3) slightly reduces fairness from 0.932 to 0.912 due to channel reuse among distant UAVs, while the complete algorithm V4 raises it to 0.977 through power adjustment and QoS-aware position optimization.

(5) Acceptable computational overhead. Despite the additional complexity of frequency allocation and power control, the computational overhead remains acceptable (+3.4 s, +27.6% increase over TLK-VNS-K), enabling practical deployment in time-sensitive emergency response scenarios. The overall time complexity is $O(I_{\text{VNS}} \cdot k_{\max} \cdot I_{\text{pc}} \cdot NK)$, which scales linearly with the number of users K and remains tractable for the emergency communication scenarios considered.

Limitations and Future Work

This study assumes predetermined CA locations and static ground users. Several promising research directions emerge for future investigation:

(1) Joint CA–UAV optimization and CA-placement sensitivity. The present work selects CA locations from predetermined candidate sites and then optimizes UAV deployment; a natural extension is to jointly optimize CA siting together with QoS-aware UAV deployment, and to systematically analyze the sensitivity of network performance to CA placement. Recent advances in facility location optimization [30] and bilevel programming [31] provide potential methodological foundations.

(2) Dynamic deployment with user mobility. Extending to mobile user scenarios with UAV trajectory planning. Deep reinforcement learning approaches [32] and model predictive control methods [33] offer promising solutions for real-time adaptation.

(3) Energy-efficient deployment. Incorporating UAV energy consumption and battery constraints into the optimization objective. Energy-aware path planning [34] and wireless power transfer techniques [35] represent relevant research directions.

(4) Learning-based online optimization. Exploring deep reinforcement learning (DRL) for online decision making without requiring complete channel state information. Recent works on multi-agent DRL for UAV networks [36] and graph neural network-based resource allocation [37] demonstrate the potential of data-driven approaches.

(5) Space–air–ground integrated networks. Extending to satellite–HAP–UAV cooperative networks for ultra-wide-area emergency coverage. Nonterrestrial network integration [38] and heterogeneous network coordination [39] provide relevant architectural frameworks.

Author Contributions: Conceptualization, C.W., L.Z. and J.L.; methodology, L.Z.; software, L.Z.; formal analysis, L.Z.; writing—original draft, L.Z.; writing—review and editing, C.W., L.Z., J.L. and S.D.; visualization, L.Z.; supervision, C.W.; project administration, C.W.; funding acquisition, C.W. All authors have read and agreed to the published version of the manuscript.

Funding: This work was funded by the National Natural Science Foundation of China, grant number 71403225; the Sichuan Provincial Natural Science Foundation, grant number 2026YFHZ0142; the Civil Aviation Airport Intelligent Operation and Maintenance Sichuan Provincial Engineering Research Center Project, project number XYKY2024003; and the Fundamental Research Funds for the Central Universities, grant number 24CAFUC04013.

Data Availability Statement: The data supporting this study are not publicly available due to legal restrictions.

Conflicts of Interest: The authors declare no conflicts of interest.

Abbreviations

The following abbreviations are used in this manuscript:

A2A	Air-to-Air
A2G	Air-to-Ground
CA	Capsule Airport
FANET	Flying Ad Hoc Network
LoS	Line-of-Sight
MILP	Mixed-Integer Linear Programming
MINLP	Mixed-Integer Nonlinear Programming
NLoS	Non-Line-of-Sight
PSO	Particle Swarm Optimization
QoS	Quality of Service
SINR	Signal-to-Interference-plus-Noise Ratio
TLK	Two-Layer K-means
U2C	UAV-to-Capsule Airport
UAV	Unmanned Aerial Vehicle
VNS	Variable Neighborhood Search

References

1. Ministry of Industry and Information Technology, China. Over 70% of Disrupted Base Stations in Henan and Zhengzhou Restored. 2021. Available online: https://www.miit.gov.cn/xwdt/gxdt/sjdt/art/2021/art_19be7c2ea024409ab2214c6a10193332.html (accessed on 23 July 2021).
2. Zeng, Y.; Zhang, R.; Lim, T.J. Wireless communications with unmanned aerial vehicles: Opportunities and challenges. *IEEE Commun. Mag.* **2016**, *54*, 36–42. [CrossRef]
3. Hayat, S.; Yanmaz, E.; Muzaffar, R. Survey on Unmanned Aerial Vehicle Networks for Civil Applications: A Communications Viewpoint. *IEEE Commun. Surv. Tutor.* **2016**, *18*, 2624–2661. [CrossRef]
4. Mozaffari, M.; Saad, W.; Bennis, M.; Nam, Y.H.; Debbah, M. A Tutorial on UAVs for Wireless Networks: Applications, Challenges, and Open Problems. *IEEE Commun. Surv. Tutor.* **2019**, *21*, 2334–2360. [CrossRef]
5. Zhao, H.; Wang, H.; Wu, W.; Wei, J. Deployment Algorithms for UAV Airborne Networks Toward On-Demand Coverage. *IEEE J. Sel. Areas Commun.* **2018**, *36*, 2015–2031. [CrossRef]
6. Li, Y.; Guo, D.; Luo, L.; Xia, M. Air-to-Ground Communications Beyond 5G: CoMP Handoff Management in UAV Network. *IEEE Trans. Wirel. Commun.* **2024**, *23*, 18822–18837. [CrossRef]
7. Hua, B.; Han, L.; Deng, Q.; Zhu, Q.; Li, H.; Qu, Y.; Briso-Rodríguez, C.; Mao, K. AAV Air-to-Air Channel: Statistical Properties and Experimental Verification. *IEEE Internet Things J.* **2025**, *12*, 25790–25803. [CrossRef]
8. Jin, X.; Luo, Z.; Shi, J.; Wang, L. Two-Layer Intelligent Deployment of Capsule Airports and Unmanned Aerial Vehicles for Providing Emergency Communication Services. *Expert Syst. Appl.* **2024**, *238*, 121795. [CrossRef]
9. Mozaffari, M.; Saad, W.; Bennis, M.; Debbah, M. Efficient Deployment of Multiple Unmanned Aerial Vehicles for Optimal Wireless Coverage. *IEEE Commun. Lett.* **2016**, *20*, 1647–1650. [CrossRef]
10. Al-Hourani, A.; Kandeepan, S.; Jamalipour, A. Modeling air-to-ground path loss for low altitude platforms in urban environments. In Proceedings of the 2014 IEEE Global Communications Conference, Austin, TX, USA, 8–12 December 2014; pp. 2898–2904. [CrossRef]
11. Al-Hourani, A.; Kandeepan, S.; Lardner, S. Optimal LAP Altitude for Maximum Coverage. *IEEE Wirel. Commun. Lett.* **2014**, *3*, 569–572. [CrossRef]
12. Alzenad, M.; El-Keyi, A.; Lagum, F.; Yanikomeroglu, H. 3-D Placement of an Unmanned Aerial Vehicle Base Station (UAV-BS) for Energy-Efficient Maximal Coverage. *IEEE Wirel. Commun. Lett.* **2017**, *6*, 434–437. [CrossRef]
13. Zeng, Y.; Zhang, R. Energy-Efficient UAV Communication With Trajectory Optimization. *IEEE Trans. Wirel. Commun.* **2017**, *16*, 3747–3760. [CrossRef]
14. Wang, L.; Zhang, H.; Guo, S.; Yuan, D. Deployment and Association of Multiple UAVs in UAV-Assisted Cellular Networks with the Knowledge of Statistical User Position. *IEEE Trans. Wirel. Commun.* **2022**, *21*, 6553–6567. [CrossRef]

15. Lyu, J.; Zeng, Y.; Zhang, R.; Lim, T.J. Placement Optimization of UAV-Mounted Mobile Base Stations. *IEEE Commun. Lett.* **2017**, *21*, 604–607. [CrossRef]
16. Sharma, V.; Bennis, M.; Kumar, R. UAV-Assisted Heterogeneous Networks for Capacity Enhancement. *IEEE Commun. Lett.* **2016**, *20*, 1207–1210. [CrossRef]
17. Premkumar, G.R.V.; Van Scoy, B. Optimal Positioning of Unmanned Aerial Vehicle (UAV) Base Stations Using Mixed-Integer Linear Programming. *Drones* **2025**, *9*, 44. [CrossRef]
18. Shi, R.; Yu, X.; Wang, Y.; Tian, Y.; Liu, Z.; Wu, W.; Zhang, X.P.; Veloso, M.M. Symmetry-Informed MARL: A Decentralized and Cooperative UAV Swarm Control Approach for Communication Coverage. *IEEE Trans. Mob. Comput.* **2025**, *24*, 8039–8056. [CrossRef]
19. Huang, H.; Savkin, A.V. A Method for Optimized Deployment of Unmanned Aerial Vehicles for Maximum Coverage and Minimum Interference in Cellular Networks. *IEEE Trans. Ind. Inform.* **2019**, *15*, 2638–2647. [CrossRef]
20. Hydher, H.; Jayakody, D.N.; Hemachandra, K.; Samarasinghe, T. Intelligent UAV Deployment for a Disaster-Resilient Wireless Network. *Sensors* **2020**, *20*, 6140. [CrossRef] [PubMed]
21. Shao, X.; Wang, W.; Zhou, B.; Pan, G.; Jiang, W. Joint Bandwidth and Spectrum Usage Zones Flexible Allocation for Coexisting Multiple UAV Networks: An Interference Graph Approach. *IEEE Internet Things J.* **2025**, *12*, 31141–31153. [CrossRef]
22. Qiu, J.; Grace, D.; Ding, G.; Zakaria, M.D.; Wu, Q. Air-Ground Heterogeneous Networks for 5G and Beyond via Integrating High and Low Altitude Platforms. *IEEE Wirel. Commun.* **2019**, *26*, 140–148. [CrossRef]
23. Kalantari, E.; Yongacoglu, A. On the Number and 3D Placement of Drone Base Stations in Wireless Cellular Networks. *arXiv* **2018**, arXiv:1804.08415. [CrossRef]
24. Alsamhi, S.H.; Shvetsov, V.A.; Kumar, S.; Shvetsova, V.S.; Alhartomi, M.A.; Hawbani, A.; Rajput, N.S.; Srivastava, S.; Saif, A.; Nyangaresi, V.O. UAV Computing-Assisted Search and Rescue Mission Framework for Disaster and Harsh Environment Mitigation. *Drones* **2022**, *6*, 154. [CrossRef]
25. Shah, A.F.M.S. Architecture of Emergency Communication Systems in Disasters through Uavs in 5G and Beyond. *Drones* **2023**, *7*, 25. [CrossRef]
26. Loor-Duque, J.J.; Castro-Arias, S.; Astudillo León, J.P.; Zambrano-Caicedo, C.J.; Reyes-Chacón, I.G.; Vizcaíno, P.; Cárdenas, L.L.; Morocho-Cayamcela, M.E. Lightweight Machine Learning-Based QoS Optimization for Multi-UAV Emergency Communications in FANETs. *Drones* **2026**, *10*, 336. [CrossRef]
27. Ehsan, S.S.; Hossain, M.S.; Ar Rafi, R.A.; Barua, S.; Haque, R. Optimizing K-Means for the Deployment of UAV-Assisted Wireless Networks: A Parametric Analysis. In Proceedings of the 2024 IEEE International Conference on Signal Processing, Information, Communication and Systems (SPICSCON), Khulna, Bangladesh, 1–2 November 2024; pp. 1–5. [CrossRef]
28. Jia, Y.; Zhou, S.; Zeng, Q.; Li, C.; Chen, D.; Zhang, K.; Liu, L.; Chen, Z. The UAV Path Coverage Algorithm Based on the Greedy Strategy and Ant Colony Optimization. *Electronics* **2022**, *11*, 2667. [CrossRef]
29. Liu, S. An Improved Particle Swarm Algorithm for UAV Path Planning. In Proceedings of the 2023 IEEE International Conference on Image Processing and Computer Applications (ICIPCA), Changchun, China, 11–13 August 2023; pp. 949–953. [CrossRef]
30. Li, F.; Li, B. Deployment Strategy of UAV Aerial Base Stations Based on Three-Dimensional Coverage Optimization. In Proceedings of the 2025 IEEE/CIC International Conference on Communications in China (ICCC), Shangai, China, 10–13 August 2025; pp. 1–6. [CrossRef]
31. Liu, W.; Wang, X.; Xu, Y. Bilevel Planning of Wireless Charging Lanes in Coupled Transportation and Power Distribution Networks. *IEEE Trans. Transp. Electrif.* **2024**, *10*, 2499–2510. [CrossRef]
32. Cheng, S.; Lin, X.; Li, X.; Wang, J. Joint UAV Trajectory and RadCom Task Schedule for IVNs: A Game-Embedding Multi-Agent Deep Reinforcement Learning Approach. *IEEE Trans. Wirel. Commun.* **2025**, *24*, 181–196. [CrossRef]
33. Chen, Q.; Jin, Y.; Wang, T.; Wang, Y.; Yan, T.; Long, Y. UAV Formation Control under Communication Constraints Based on Distributed Model Predictive Control. *IEEE Access Pract. Innov. Open Solut.* **2022**, *10*, 126494–126507. [CrossRef]
34. Liu, T.; Sun, C.; Zhang, Y.; Sun, W. Energy-Efficient End-to-End Optimization for UAV-assisted IoT Data Collection and LEO Satellite Offloading in SAGIN. *Electronics* **2025**, *15*, 24. [CrossRef]
35. Shi, J.; Yang, Q.; Zhao, L.; Cong, P.; Bi, Y.; Hawbani, A. Energy-Efficient UAV-enabled Wireless Power Transfer for Real-Time Charging Requirements. In *Proceedings of the Advanced Intelligent Computing Technology and Applications, Pt Ii, Icic, Tianjin, China, 5–8 August 2024*; Lecture Notes in Artificial Intelligence; Huang, D.S., Zhang, C., Pan, Y., Eds.; Springer: Singapore, 2024; Volume 14876, pp. 356–367. [CrossRef]
36. Zhao, N.; Ye, Z.; Pei, Y.; Liang, Y.C.; Niyato, D. Multi-Agent Deep Reinforcement Learning for Task Offloading in UAV-Assisted Mobile Edge Computing. *IEEE Trans. Wirel. Commun.* **2022**, *21*, 6949–6960. [CrossRef]
37. Ji, M.; Wu, Q.; Fan, P.; Cheng, N.; Chen, W.; Wang, J.; Letaief, K.B. Graph Neural Networks and Deep Reinforcement Learning-Based Resource Allocation for V2X Communications. *IEEE Internet Things J.* **2025**, *12*, 3613–3628. [CrossRef]

38. Heydarishahreza, N.; Han, T.; Ansari, N. Spectrum Sharing and Interference Management for 6G LEO Satellite-Terrestrial Network Integration. *IEEE Commun. Surv. Tutor.* **2025**, *27*, 2794–2825. [CrossRef]
39. Chen, C.; Zhang, T.; Xu, W.; Yang, X.; Wang, Y. Multi-UAV Cooperation Based Edge Computing Offloading in Emergency Communication Networks. In Proceedings of the 2023 IEEE Wireless Communications and Networking Conference (WCNC), Glasgow, UK, 26–29 March 2023; pp. 1–6. [CrossRef]

Disclaimer/Publisher's Note: The statements, opinions and data contained in all publications are solely those of the individual author(s) and contributor(s) and not of MDPI and/or the editor(s). MDPI and/or the editor(s) disclaim responsibility for any injury to people or property resulting from any ideas, methods, instructions or products referred to in the content.